

See discussions, stats, and author profiles for this publication at: <https://www.researchgate.net/publication/235290314>

# Chlorophyll a algorithms for oligotrophic oceans: A novel approach based on three-band reflectance difference

Article in *Journal of Geophysical Research Atmospheres* · January 2012

DOI: 10.1029/2011JC007395

---

CITATIONS

788

READS

2,368

3 authors, including:



Bryan A Franz

NASA Goddard Space Flight Center, Greenbelt, MD, United States

210 PUBLICATIONS 11,323 CITATIONS

SEE PROFILE

# Chlorophyll *a* algorithms for oligotrophic oceans: A novel approach based on three-band reflectance difference

Chuanmin Hu,<sup>1</sup> Zhongping Lee,<sup>2</sup> and Bryan Franz<sup>3</sup>

Received 18 June 2011; revised 22 October 2011; accepted 9 November 2011; published 20 January 2012.

[1] A new empirical algorithm is proposed to estimate surface chlorophyll *a* (Chl) concentrations in the global ocean for Chl  $\leq 0.25 \text{ mg m}^{-3}$  ( $\sim 78\%$  of the global ocean area). The algorithm is based on a color index (CI), defined as the difference between remote-sensing reflectance ( $R_{rs}$ ,  $\text{sr}^{-1}$ ) in the green and a reference formed linearly between  $R_{rs}$  in the blue and red. For low-Chl waters, in situ data showed a tighter (and therefore better) relationship between CI and Chl than between traditional band ratios and Chl, which was further validated using global data collected concurrently by ship-borne and Sea-viewing Wide Field-of-view Sensor (SeaWiFS) and Moderate Resolution Imaging Spectroradiometer (MODIS)/Aqua instruments. Model simulations showed that for low-Chl waters, compared with the band-ratio algorithm, the CI-based algorithm (CIA) was more tolerant to changes in chlorophyll-specific backscattering coefficient and performed similarly for different relative contributions of nonphytoplankton absorption. Simulations using existing atmospheric correction approaches further demonstrated that the CIA was much less sensitive than band-ratio algorithms to various errors induced by instrument noise and imperfect atmospheric correction (including sun glint and whitecap corrections). Image and time series analyses of SeaWiFS and MODIS/Aqua data also showed improved performance in terms of reduced image noise, more coherent spatial and temporal patterns, and better consistency between the two sensors. The reduction in noise and other errors is particularly useful to improve the detection of various ocean features such as eddies. Preliminary tests over Medium-Resolution Imaging Spectrometer and Coastal Zone Color Scanner data indicate that the new approach should be generally applicable to all past, current, and future ocean color instruments.

**Citation:** Hu, C., Z. Lee, and B. Franz (2012), Chlorophyll *a* algorithms for oligotrophic oceans: A novel approach based on three-band reflectance difference, *J. Geophys. Res.*, 117, C01011, doi:10.1029/2011JC007395.

## 1. Introduction

[2] Over the past half century, algorithms to invert ocean color (i.e., spectral radiance or reflectance of the surface ocean) to phytoplankton chlorophyll *a* (Chl) concentrations (in  $\text{mg m}^{-3}$ ) have evolved from simple empirical regressions [Gordon and Morel, 1983] to semianalytical inversions based on radiative transfer theory (Sathyendranath *et al.* [1989], Carder *et al.* [1999], Maritorena *et al.* [2002], and others). While each of these approaches has its own advantages and disadvantages (and thus applicability range), an algorithm based on a spectral ratio of remote-sensing reflectance ( $R_{rs}$ ,  $\text{sr}^{-1}$ ) historically has been used as the default algorithm formulation to produce global chlorophyll-*a*

products from measurements made by satellite instruments. These include the Coastal Zone Color Scanner (CZCS; 1978–1986), the Sea-viewing Wide Field-of-view Sensor (SeaWiFS; 1997–2010), and the Moderate Resolution Imaging Spectroradiometer (MODIS; 1999 to the present for the Terra satellite and 2002 to the present for the Aqua satellite). The current default Chl algorithm for SeaWiFS and MODIS is based on the OCx form of O'Reilly *et al.* [2000], with coefficients derived using in situ data from the NASA bio-Optical Marine Algorithm Data set (NOMAD) version 2 (<http://oceancolor.gsfc.nasa.gov/REPROCESSING/R2009/ocv6/>). The default SeaWiFS algorithm is referred to as OC4 in this paper. Correspondingly, many large-scale studies of ocean carbon cycles and biogeochemistry that utilized satellite ocean color data, from regional and basin to global scale, have used the OC4 data products [e.g., Gregg *et al.*, 2005; Behrenfeld *et al.*, 2006; Yoder and Kennelly, 2006; Polovina *et al.*, 2008], leading to documented changes in Chl<sub>OC4</sub> and primary productivity at various spatial/temporal scales and connections to climate variability.

[3] An early review on the history of the band-ratio empirical algorithms, as well as their advantages and

<sup>1</sup>College of Marine Science, University of South Florida, St. Petersburg, Florida, USA.

<sup>2</sup>Department of Environmental, Earth and Ocean Sciences, University of Massachusetts, Boston, Massachusetts, USA.

<sup>3</sup>NASA GSFC, Greenbelt, Maryland, USA.

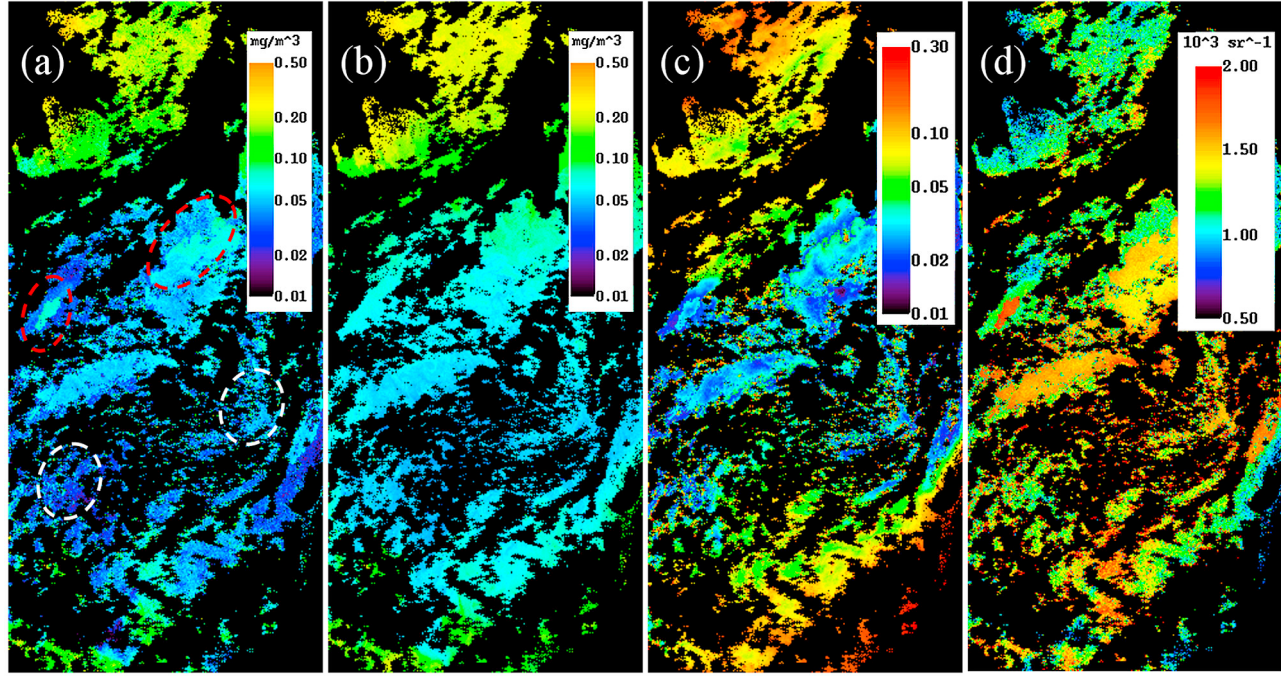


**Figure 1.** SeaWiFS Level-2 GAC data products at 4 km resolution on 20 February 1998 over the Sargasso Sea (about  $1800 \times 2640$  km centered at  $25.5^\circ\text{N}$ ,  $54.8^\circ\text{W}$ ). (a) Chl derived from the default OC4v6 algorithm ( $\text{Chl}_{\text{OC}4}$ ). (b) Chl derived from a new CI-based algorithm ( $\text{Chl}_{\text{CI}}$ ; see text for details). (c) Aerosol optical thickness at 865 nm ( $\tau_{865}$ , dimensionless). (d) Remote-sensing reflectance at 555 nm ( $R_{\text{rs}}(555)$ ,  $\times 10^3 \text{ sr}^{-1}$ ). All suspicious data, as defined by the various Level-2 flags, have already been removed (black color). Note the speckling noise (white circles) and patchiness (red circles) shown in Figure 1a.

disadvantages, was provided by *Gordon and Morel* [1983] and recently revisited by *Dierssen* [2010]. Briefly, the most recent OC4v6 algorithm evolved from its predecessors in the 1970s and 1980s [*Clarke et al.*, 1970; *Arvesen et al.*, 1973; *Hovis and Leung*, 1977; *Clark et al.*, 1980; *Gordon and Clark*, 1980; *Morel*, 1980], when the radiance ratio of blue and green wavelengths was recognized to correlate well with surface Chl. The underlying assumption is that the relative changes between the blue and green bands are primarily driven by changes in phytoplankton and their direct degradation products (i.e., the traditional case I scenario [see *Morel and Prieur*, 1977]), and the latter can therefore be inferred from the former. Indeed, despite the various studies showing the algorithm artifacts in non-case I (i.e., case II) waters (e.g., *Dierssen et al.* [2002], *Hu et al.* [2003], *Odriozola et al.* [2007], and others), global validation efforts of the SeaWiFS  $\text{Chl}_{\text{OC}4}$  data products proved that for most open ocean waters, the algorithm performed well, with RMS differences from ship-based Chl (after logarithmic transformation) of 0.2–0.3 without significant bias [*Gregg and Casey*, 2004; *McClain et al.*, 2004a; *McClain*, 2009]. Agreement/disagreement varied among different ocean basins because the same regression coefficients, determined from the global data set optimization, were applied universally [*Gregg and Casey*, 2004]. To address these regional differences, various band combinations and regression coefficients were developed for different water types [e.g., *Kahru and Mitchell*, 1999; *McKee et al.*, 2007; *Mitchell and Kahru*, 2009], with similar band-ratio forms.

[4] All previous global-scale studies used spatially and temporally composited data (e.g., monthly composites at reduced resolution) to reduce data volume and fill in data gaps due to cloud cover and other measurement/algorithm artifacts. Chl data product errors at original spatial and temporal resolutions are smoothed and smeared in these higher-level data products, thus complicating the propagation of errors to trend/variability analyses at global or regional scales. These errors are particularly evident at low concentrations ( $\text{Chl} < 0.1 \text{ mg m}^{-3}$ ). Figure 1a shows a typical example of the SeaWiFS global area coverage (GAC) Level-2 Chl data product for the Sargasso Sea, an oligotrophic ocean gyre in the North Atlantic. Due to a variety of reasons (see details below), the image shows patchiness and speckle noise (pixelization) and is not spatially coherent. Note that all nonzero Chl values in this image are regarded as acceptable quality and used in composing the higher-level (i.e., lower spatial and temporal resolution) products, because all low-quality data, as defined by the various quality flags, are already discarded. The image was selected rather arbitrarily for demonstration purposes, and similar problems could be visualized in almost every Level-2 GAC image. Clearly, these issues need to be addressed in order to understand how they may propagate to higher-level products to affect the large-scale trend/variability analyses.

[5] Recently, in response to the Deepwater Horizon (DWH) oil spill disaster in the northeastern Gulf of Mexico and to derive spatially coherent and temporally consistent ocean color patterns from satellite images contaminated by

severe sun glint, a new color index (CI) was developed for satellite ocean color observations [Hu, 2011]. Instead of using a blue-green band ratio as the independent variable, the CI is calculated as the difference between the green-band reflectance and a reference formed linearly by the blue and red bands. This is similar to the design of the MODIS fluorescence line height [Letelier and Abbott, 1996] and Medium-Resolution Imaging Spectrometer (MERIS) maximal chlorophyll index [Gower et al., 2005], except that the bands are shifted to blue-green-red. Hu [2009] used a similar form to detect and quantify the reflectance peak in the MODIS 859 nm band and proved that the floating algae index (FAI), derived using the 645–859–1240 band combination, was much less sensitive to variable observing conditions (aerosols, sun glint, thin clouds, solar/viewing geometry) than band-ratio algorithms. The MODIS CI appears to be relatively insensitive to residual errors due to imperfect empirical glint correction, and in glint-free areas, it is also well correlated with MODIS band-ratio Chl [Hu, 2011], suggesting that a new Chl algorithm might be developed to remove residual atmosphere correction-related errors and image noise.

[6] Inspired by these recent works, a new empirical algorithm to retrieve Chl using the CI as the independent variable is developed and validated in this paper. Using data collected primarily by both SeaWiFS and MODIS/Aqua, as well as other satellite instruments, we evaluate the performance of such a band-difference algorithm (i.e., the CI algorithm or CIA) compared with the OCx band-ratio algorithms. We demonstrate and argue that because the CI is much more tolerant than the band ratio to various perturbations in sensor hardware and data processing (e.g., instrument noise, residual errors in atmospheric correction, whitecap and sun glint corrections, stray light contamination), and also more tolerant to perturbations of Chl-independent particle backscattering from the water column, the CIA is superior to band-ratio algorithms in deriving a more consistent and accurate Chl climate data record for most oligotrophic oceans.

[7] This paper is arranged as follows. The principles to “measure” Chl from space, although found in the refereed literature, are briefly introduced for the reader’s convenience. The in situ and satellite data used to develop and validate the new algorithm are then described. Following that, the new Chl algorithm (CIA) is described and validated for SeaWiFS and MODIS/Aqua. Its sensitivity to errors and perturbations, compared with the OC4 algorithm, is analyzed in detail and further demonstrated using satellite measurements. Sample time series at several arbitrarily selected oligotrophic ocean sites as well as from global-scale data are used to evaluate the performance of the new algorithm. Finally, we discuss the new algorithm’s applicability to other satellite instruments such as MERIS and CZCS and discuss its potential to improve data quality, time series and cross-sensor consistency, and image quality in feature detection.

## 2. Principles to “Measure” Chl From Space

[8] A multiband ocean-color satellite instrument measures the top-of-atmosphere radiance or reflectance in several spectral bands covering the visible to the near-infrared domain. On SeaWiFS, the spectral bands are centered at  $\lambda = 412, 443, 490, 510, 555, 670, 765$ , and 865 nm. On

MODIS/Aqua, they are centered at  $\lambda = 412, 443, 488, 531, 547, 667, 678, 748$ , and 869 nm. After radiometric calibration (including in-orbit vicarious calibration [Franz et al., 2007]) the calibrated at-sensor reflectance ( $\rho_t(\lambda)$ ), after accounting for the effects of ozone and other gaseous absorption, is used to derive the at-sea remote-sensing reflectance ( $R_{rs}$ ) [Gordon, 1997]. With some simplifications, this can be expressed as

$$\begin{aligned} \rho_t(\lambda) &= \rho_r(\lambda) + \rho_{ar}(\lambda) + t(\lambda)\rho_{wc}(\lambda) + T(\lambda)\rho_g(\lambda) \\ &\quad + \pi t(\lambda)t_0(\lambda)R_{rs}(\lambda), \end{aligned} \quad (1)$$

where  $\rho_r$  is that due to Rayleigh scattering;  $\rho_{ar}$  is that due to aerosol scattering and aerosol-Rayleigh interactions;  $\rho_{wc}$  is the whitecap reflectance;  $\rho_g$  is the sun-glint reflectance;  $T$  and  $t$  are the direct and diffuse transmittance from the target (pixel of the imagery) to the sensor (satellite), respectively; and  $t_0$  is the diffuse transmittance from the sun to the target.

[9] Deriving  $R_{rs}(\lambda)$  from  $\rho_t(\lambda)$  is through a sophisticated atmospheric correction, which uses lookup tables for aerosol and molecular properties [Gordon and Wang, 1994a, 1994b; Ahmad et al., 2010; Bailey et al., 2010] after removing contributions from whitecaps [Frouin et al., 1996] and sun glint [Wang and Bailey, 2001]. The retrieved  $R_{rs}(\lambda)$  is then used as the input to an established bio-optical inversion model to derive Chl. For the OC4 algorithm applied to SeaWiFS, where “4” stands for four bands, Chl is derived as [O'Reilly et al., 2000]

$$\begin{aligned} \text{Chl}_{\text{OC4}} &= 10^y \\ y &= a_0 + a_1 \chi + a_2 \chi^2 + a_3 \chi^3 + a_4 \chi^4 \\ \chi &= \log_{10}(R) \text{ and } R = \max(R_{rs}(443, 490, 510))/R_{rs}(555), \end{aligned} \quad (2)$$

where  $a_0 - a_4$  are the empirical regression coefficients, for which the current values (version 6) are 0.3272, -2.9940, 2.7218, -1.2259, and -0.5683, respectively. For the OC3 algorithm applied to MODIS,  $R$  is defined as  $\max(R_{rs}(443, 488))/R_{rs}(547)$ , with regression coefficients adjusted to represent the best fit between  $R$  and Chl.

[10] The algorithm details and their performance at global and regional scales can be found in the published literature as well as in online documents (<http://oceancolor.gsfc.nasa.gov/REPROCESSING/R2009/ocv6/>).

## 3. Data Sources Used in This Study

[11] In situ data were obtained from the NASA SeaWiFS Bio-optical Archive and Storage System (SeaBASS) archive, which is a database of measurements collected by many research groups in order to develop and validate satellite ocean-color algorithms. The NOMAD data set, described by Werdell and Bailey [2005], is a subset of SeaBASS specifically compiled for bio-optical algorithm development, as it contains coincident measurements of Chl,  $R_{rs}(\lambda)$ , and other data collected simultaneously in the global oceans.

[12] Like the current OC4 algorithm, the data set used to develop the CIA was taken from NOMAD version 2, covering a period of 1991–2007 and containing 4459 data records. Similar to Morel et al. [2007a], the NOMAD data used in the present study for algorithm development are those with Chl determined via high-performance liquid

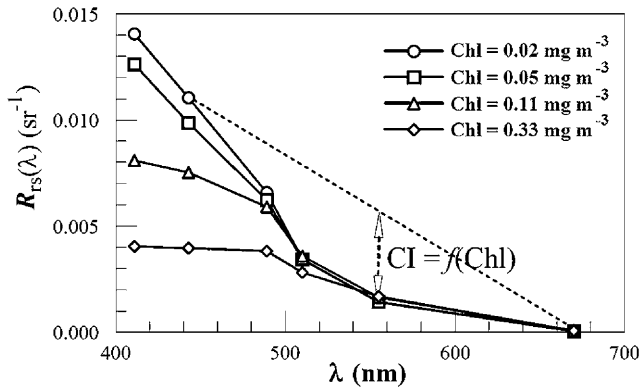


**Figure 2.** Illustration of the CI algorithm concept. When Chl increases from 0.02 to  $0.33 \text{ mg m}^{-3}$ ,  $R_{\text{rs}}(443)$  decreases while  $R_{\text{rs}}(555)$  and  $R_{\text{rs}}(670)$  remain relatively stable. Thus, the distance from  $R_{\text{rs}}(555)$  to the linear baseline between  $R_{\text{rs}}(443)$  and  $R_{\text{rs}}(670)$  (dotted line in the figure), defined as the CI, is highly correlated with Chl. This is the same principle as using the  $R_{\text{rs}}(443)/R_{\text{rs}}(555)$  ratio to relate to Chl. These in situ data are from the NOMAD data set.

chromatography (HPLC) because (1) for most concentrations, HPLC and fluorometric measurements agree well [Werdell and Bailey, 2005, Figure 6]; (2) for low concentrations, Chl determined from fluorometric methods often suffer from contaminations by chlorophyll *b* and chlorophyll *c*, as demonstrated from data collected in the Southern Ocean [Marrari et al., 2006; Dierssen, 2010]; and (3) the focus of this work is on clear water with low concentrations, and the NOMAD data sets contain more HPLC than fluorometric measurements for extremely clear waters ( $\text{Chl} < 0.05 \text{ mg m}^{-3}$ ). Furthermore, we applied the following criteria to select data for the oligotrophic oceans:  $R_{\text{rs}}(\lambda) > 0.0 \text{ sr}^{-1}$ ,  $\text{Chl} > 0.0 \text{ mg m}^{-3}$ , bottom depth  $>30.0 \text{ m}$ , and latitude between  $60^{\circ}\text{N}$  and  $60^{\circ}\text{S}$ . A total of 136 data records were obtained.

[13] To evaluate the algorithm performance when applied to satellite data, in situ data were also obtained from the SeaBASS archive through online query. The following criteria were used to search for the in situ-satellite matching pairs: bottom depth  $>30 \text{ m}$ ; solar zenith angle  $<70^{\circ}$ ; satellite zenith angle  $<56^{\circ}$ ; time difference between satellite and in situ measurements  $<3 \text{ h}$ ; satellite Chl variance (standard deviation divided by mean) from the  $3 \times 3$  pixels centered at the in situ stations  $<15\%$ ; difference between modeled and measured surface irradiance  $<100\%$ ; wind speed  $<35 \text{ m s}^{-1}$ . For SeaWiFS, a total of 1424 matching pairs were obtained for 1998–2010. For MODIS/Aqua, a total of 330 matching pairs were obtained for 2002–2010.

[14] The online query also resulted in the satellite Level-2 computer file names corresponding to the matching pairs. These Level-2 data products were derived by the NASA Ocean Biology Processing Group using the most recent updates in algorithms and instrument calibration (Reprocessing 2010.0, SeaDAS6.1). The data products include  $\text{Chl}_{\text{OC4}}$ , aerosol optical thickness at 865 nm ( $\tau_{865}$ ), and  $R_{\text{rs}}(\lambda)$ .  $R_{\text{rs}}(\lambda)$  data extracted from the Level-2 files were used as the input to derive  $\text{Chl}_{\text{CI}}$  (Chl from the CI algorithm) and compared with those determined from the in situ measurements.

[15] To evaluate algorithm performance in constructing time series, SeaWiFS Level-2 data between 1998 and 2010 covering two oligotrophic gyres, namely, in the Sargasso Sea ( $15\text{--}35^{\circ}\text{N}$ ,  $60\text{--}40^{\circ}\text{W}$ ) and in the eastern South Pacific Gyre ( $20\text{--}40^{\circ}\text{S}$ ,  $120\text{--}100^{\circ}\text{W}$ ), were obtained from the NASA Goddard Space Flight Center. For cross-sensor consistency evaluations, SeaWiFS and MODIS/Aqua Level-3 global daily data for 2006 were used. Some Level-2 data files from MODIS/Aqua, MERIS, and CZCS covering the western North Atlantic Sea were also used for algorithm evaluation.

#### 4. The New Empirical Chl Algorithm

[16] Similar to the MODIS CI derived from the Rayleigh-corrected reflectance [Hu, 2011], the  $R_{\text{rs}}$ -based SeaWiFS CI is defined as the relative height of  $R_{\text{rs}}(555)$  from a background, i.e., difference between  $R_{\text{rs}}(555)$  and a baseline formed linearly between  $R_{\text{rs}}(443)$  and  $R_{\text{rs}}(670)$  (Figure 2):

$$\text{CI} = R_{\text{rs}}(555) - [R_{\text{rs}}(443) + (555-443)/(670-443) * (R_{\text{rs}}(670) - R_{\text{rs}}(443))],$$

which is equivalent to  $\text{CI} \approx R_{\text{rs}}(555) - 0.5(R_{\text{rs}}(443) + R_{\text{rs}}(670)).$  (3)

[17] By this definition, for most clear ocean waters, CI is negative. Because for most clear waters  $R_{\text{rs}}(670)$  is negligible (see the “clear water” concept described by Gordon and Clark [1981] and revisited by Morel and Maritorena [2001]), CI is basically a weighted relative difference between  $R_{\text{rs}}(443)$  and  $R_{\text{rs}}(555)$ . Just as a ratio between the two is related to Chl, since  $R_{\text{rs}}(555)$  is relatively stable but  $R_{\text{rs}}(443)$  is sensitive to Chl changes for clear waters [Gordon and Morel, 1983], a difference between the two should also be related to Chl, and this forms the basis of the new Chl algorithm (the theoretical basis of this algorithm is provided in section 6.1 below). Indeed, Figure 2 shows that with increasing Chl, the magnitude of CI decreases monotonically. The added band at 670 nm has a great advantage in compensating various errors in atmospheric correction and other corrections when the algorithm is applied to satellite data (see below).

[18] Using the NOMAD data set, the relationships between band-ratio  $R$  and Chl (equation (2)) and between CI and Chl are shown in Figures 3a and 3b, respectively, for data collected from the 136 qualified stations. Also overlaid on Figure 3a is the OC4v6 prediction (Figure 3a, solid line), which shows that the globally optimized regression relationship fits well with the low Chl values. If a similar band-ratio form is developed using the low-concentration stations only (Figure 3a, green dots), slightly better performance can be achieved as measured by the statistics (Table 1), but at the price of sacrificing the intermediate values (Figure 3a, red line) because the numerical fit tends to plateau for Chl around 0.2 and  $0.3 \text{ mg m}^{-3}$ .

[19] The statistical measure of the algorithm performance is listed in Table 1. Note that when evaluating the relative difference between the two data sets,  $x$  and  $y$  (in this case, one is the in situ measurement ( $x$ ) and the other is the algorithm prediction ( $y$ )), RMS difference (or error) is typically evaluated using the form of  $(y - x)/x$ . However, when one data set contains substantial errors, the  $(y - x)/x$  ratio may be extremely large and therefore creates biased estimates for the relative difference. For this reason, an unbiased

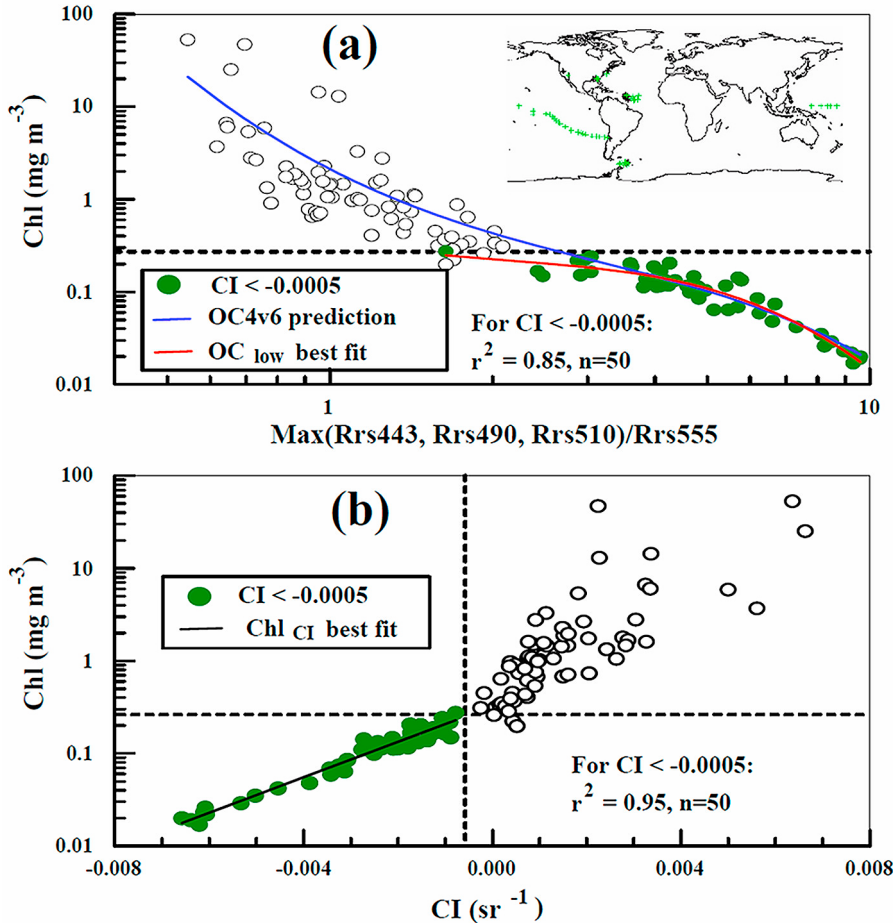


**Figure 3.** Relationship between in situ Chl and (a) reflectance ratio  $R$  and (b) CI. The highlighted points emphasize those corresponding to  $\text{CI} \leq -0.0005$ , where the corresponding data collection locations are shown in the inset map. Note that the minimum Chl in this data set is about  $0.02 \text{ mg m}^{-3}$ . In Figure 3a, the RMS error is estimated between measured and OC4v6-predicted Chl. If a best fit from all data points for  $\text{CI} < -0.0005 \text{ sr}^{-1}$  is used, RMS error is reduced to 22.95%. Statistics are presented in Table 1.

RMS was also estimated using  $(y - x)/(0.5x + 0.5y)$  [Hooker *et al.*, 2002]. And this evaluation was also used for comparison between satellite and in situ Chl data below. When the Chl data cover a large dynamic range, they tend to be lognormal [Campbell, 1995]. Thus,  $R^2$  between the log-transformed data was also estimated and presented in Table 1.

[20] Figure 3b shows that for low Chl values, there is a strong relationship between CI and Chl, confirming the visual interpretation of Figure 2. Nonlinear regression for  $\text{CI} \leq -0.0005$  resulted in a coefficient of determination ( $R^2$ ) of 0.95 ( $n = 50$ ) and a RMS difference of 16.52% between the CI-predicted Chl ( $\text{Chl}_{\text{CI}}$ ) and the measured Chl:

$$\text{Chl}_{\text{CI}} = 10^{-0.4909+191.6590*\text{CI}} [\text{CI} \leq -0.0005 \text{ sr}^{-1}]. \quad (4)$$

[21] In comparison, for the same data points corresponding to  $\text{CI} \leq -0.0005 \text{ sr}^{-1}$  ( $n = 50$ ), the OC4v6-predicted Chl showed a lower coefficient of determination ( $R^2 = 0.85$ ,  $n = 50$ ) and higher RMS difference from the in situ Chl (RMS = 34.87%). Even when new coefficients from these low-Chl data points were tuned to result in a better fit between band-ratio  $R$  and Chl, RMS difference was reduced to 22.95% but still higher than the CI predictions (Table 1).

Indeed, the contrast between the different data scattering for  $\text{Chl}_{\text{OC4}}$  (Figure 3a) and for  $\text{Chl}_{\text{CI}}$  (Figure 3b) is apparent. From this regression alone, the CIA appears to perform better than the OC4v6 for low concentrations ( $\text{Chl} \leq 0.25 \text{ mg m}^{-3}$ ). Note that although the number of data points used in the regression is limited ( $n = 50$ ), they were collected from different ocean basins (Figure 3a, inset) covering the Pacific, Atlantic, Gulf of Mexico, and Southern oceans. Thus, the CIA might be applicable to most oligotrophic waters.

**Table 1.** Chl Algorithm Performance for  $\text{CI} < -0.0005 \text{ sr}^{-1}$  Using the NOMAD Data Set<sup>a</sup>

Algorithm	RMS	URMS	Mean Ratio	Median Ratio	$R^2$ (Linear)	$R^2$ (Log)	N
OC4v6	34.9%	28.2%	1.11	1.08	0.73	0.85	50
CI	16.5%	16.2%	1.01	1.01	0.78	0.95	50
OC <sub>low</sub>	23.0%	22.3%	1.03	1.05	0.73	0.85	50

<sup>a</sup>OC<sub>low</sub> represents a local polynomial fit between the log-transformed band ratio and Chl for low concentrations only ( $\text{CI} < -0.0005$ ; Figure 3a, red line), which shows improved performance than the globally tuned OC4v6. The regression equation is  $\text{Chl}_{\text{OC\_low}} = 10^y$  and  $y = 0.3906 - 1.5479\chi + 3.2125\chi^2 - 3.1073\chi^3$ . URMS is “unbiased” RMS (see text for details).

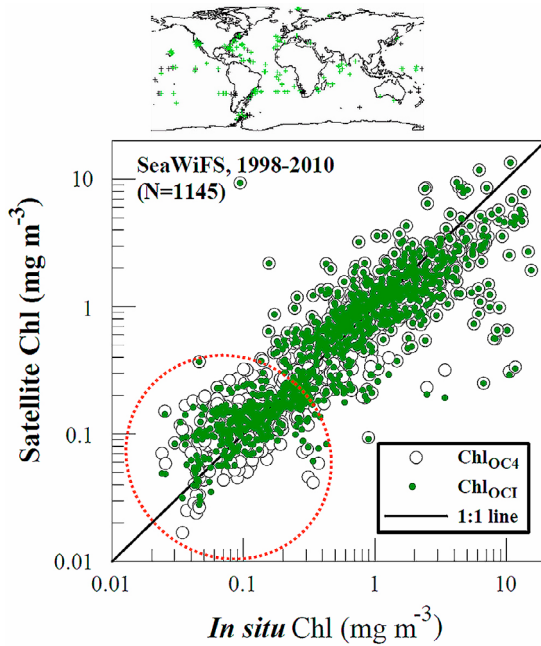


**Figure 4.** Comparison between in situ Chl and satellite-based Chl for SeaWiFS. The satellite Chl was derived from both the OC4v6 algorithm (open circles) and Ocean Color Index (OCI) algorithm (dots). Note that for  $\text{Chl} > 0.3 \text{ mg m}^{-3}$ , the results from the two algorithms were forced to be identical (equation (5)). The locations of the in situ measurements for  $\text{Chl} \leq 0.25 \text{ mg m}^{-3}$  are shown in the corresponding map. The comparison statistics for low concentration ( $\text{Chl} \leq 0.25$ ) are listed in Table 2.

[22] Figure 3b also shows that the CIA may only be applicable for low concentrations, because the relationship quickly falls apart for  $\text{CI} > 0.0005 \text{ sr}^{-1}$ , corresponding to  $\text{Chl}_{\text{CI}} \sim 0.4 \text{ mg m}^{-3}$ . The reason why the CIA does not work well above this concentration is demonstrated in sections 6.1 and 6.2 using radiative transfer modeling. Indeed, above this concentration, the CIA tends to underestimate Chl significantly (Figure 3b), where the original OC4v6 should be used instead. For intermediate concentrations, a mixture between the two algorithms may be used to assure image smoothness when the algorithm switches from one to another. For such practical considerations, the upper bound of  $0.4 \text{ mg m}^{-3}$  was lowered to  $0.3 \text{ mg m}^{-3}$  (after trial and error with image and histogram analyses to assure a smooth transition) so that CIA works even at this upper bound. Thus, the new global product of chlorophyll (Chl<sub>OCl</sub>) is defined as follows:

$$\begin{aligned} \text{Chl}_{\text{OCl}} &= \text{Chl}_{\text{CI}} [\text{for } \text{Chl}_{\text{CI}} \leq 0.25 \text{ mg m}^{-3}] \\ &= \text{Chl}_{\text{OC4}} [\text{for } \text{Chl}_{\text{CI}} > 0.3 \text{ mg m}^{-3}] \end{aligned} \quad (5)$$

$$\alpha \times \text{Chl}_{\text{OC4}} + \beta \times \text{Chl}_{\text{CI}} [\text{for } 0.25 < \text{Chl}_{\text{CI}} \leq 0.3 \text{ mg m}^{-3}],$$

where  $\alpha = (\text{Chl}_{\text{CI}} - 0.25)/(0.3 - 0.25)$  and  $\beta = (0.3 - \text{Chl}_{\text{CI}})/(0.3 - 0.25)$ . Because such derived Chl is from two algorithms (OC4 and CIA), we use the term Chl<sub>OCl</sub> hereafter to represent the merged product. Note that although the algorithm blending for Chl between  $0.25$  and  $0.3 \text{ mg m}^{-3}$  might create some artifacts in image smoothness around the lower and upper bounds ( $0.25$  and  $0.3$ ), histogram analyses

of the entire Chl range from SeaWiFS data did not show any noticeable artifacts in data continuity. On average, SeaWiFS monthly data between 1998 and 2010 showed that  $77.8 \pm 1.0\%$  of the global ocean had  $\text{Chl} \leq 0.25 \text{ mg m}^{-3}$  and  $5.06 \pm 0.43\%$  of the global ocean had Chl between  $0.25$  and  $0.3 \text{ mg m}^{-3}$ .

## 5. Validation of the New Chl Algorithm

[23] The CIA was implemented to derive Chl<sub>OCl</sub> from SeaWiFS and MODIS/Aqua Level-2  $R_{rs}(\lambda)$  data where concurrent in situ Chl were found (see data source). Because the MODIS green band is centered at  $547 \text{ nm}$  instead of  $555 \text{ nm}$  for SeaWiFS, MODIS  $R_{rs}(547)$  was converted to  $R_{rs}(555)$  by multiplying  $0.93$  according to data regression from in situ measurements in the South Pacific (not shown). Figure 4 shows the comparison between in situ Chl and SeaWiFS Chl<sub>OCl</sub> and between in situ Chl and SeaWiFS Chl<sub>OC4</sub>. Similarly, Figure 5 shows the comparison between in situ Chl and MODIS/Aqua Chl<sub>OCl</sub> and between in situ Chl and MODIS/Aqua Chl<sub>OC3</sub>. For high concentrations ( $\text{Chl}_{\text{OCl}} > 0.3 \text{ mg m}^{-3}$ ), the data points between the two

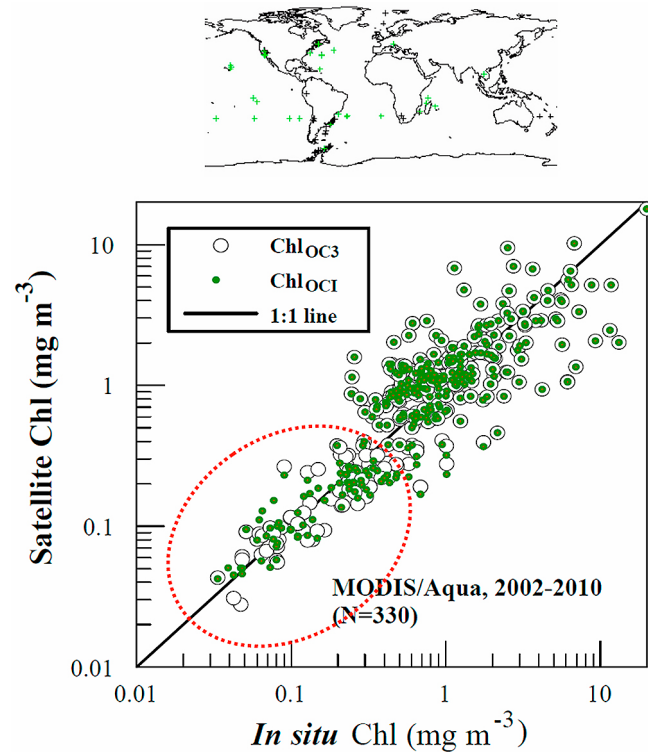


**Figure 5.** Comparison between in situ Chl and satellite-based Chl for MODIS/Aqua. The satellite Chl was derived from both the OC3 algorithm (open circles) and OCI algorithm (dots). For algorithm consistency, MODIS  $R_{rs}(547)$  was converted to  $R_{rs}(555)$  by  $R_{rs}(555) = 0.93 R_{rs}(547)$  according to in situ data collected from the South Pacific (not shown here). Note that for  $\text{Chl} > 0.3 \text{ mg m}^{-3}$ , the results from the two algorithms were forced to be identical (equation (5)). The locations of the in situ measurements for  $\text{Chl} \leq 0.25 \text{ mg m}^{-3}$  are shown in the corresponding map. The comparison statistics for low concentration ( $\text{Chl} \leq 0.25 \text{ mg m}^{-3}$ ) are listed in Table 3.

**Table 2.** Chl Algorithm Performance From SeaWiFS Measurements for Chl  $\leq 0.25 \text{ mg m}^{-3}$ , as Gauged by in Situ Chl<sup>a</sup>

Algorithm	RMS	URMS	Mean Ratio	Median Ratio	MRE	$R^2$ (Linear)	$R^2$ (Log)	$N$
OC4v6	535.8%	54.2%	1.79	1.19	41.5%	0.01	0.33	357
CI	91.8%	47.2%	1.40	1.16	36.8%	0.31	0.39	357
OC <sub>low</sub>	92.9%	45.6%	1.33	1.08	34.7%	0.20	0.36	357

<sup>a</sup>SeaWiFS-derived  $R_{rs}(\lambda)$  were used as the input of all algorithms. OC<sub>low</sub> represents a local band-ratio algorithm for low concentrations only (CI <  $-0.0005 \text{ sr}^{-1}$ ; Figure 3a, red line). URMS, “unbiased” RMS (see text for details); MRE, mean relative error after converting negative errors to positive.

algorithms were forced to be identical (equation (5)). For low concentrations (Chl  $\leq 0.25 \text{ mg m}^{-3}$ ), the CI algorithm outperforms the OC4 (SeaWiFS; Table 2) and OC3 (MODIS/Aqua; Table 3) algorithms by all measures, from RMS difference,  $R^2$ , to mean and median ratios. Note that although only a limited number of data points were available for low concentrations, a slight improvement in algorithm performance may lead to larger difference in image analysis, because the majority of the ocean is oligotrophic. Indeed, analysis of the 13 year SeaWiFS monthly data between 1998 and 2010 indicated that  $77.8 \pm 1.0\%$  of the global ocean waters had surface Chl  $\leq 0.25 \text{ mg m}^{-3}$  and  $82.9 \pm 1.4\%$  had surface Chl  $\leq 0.3 \text{ mg m}^{-3}$ . Thus, such a new algorithm might have profound effects on global- and basin-scale studies. Note that if a local OCx algorithm is developed for low concentrations only (Figure 3a, red line), its performance for SeaWiFS data will also improve over the globally tuned OC4 algorithm in statistical measures and is also slightly better than the CIA in terms of median ratio. How-

corrected [Morel and Gentili, 1993; Lee et al., 2011],  $R_{rs}(\lambda)$  is entirely determined by the inherent optical properties (IOPs) through primarily spectral absorption and backscattering by the various in-water optically active constituents (OACs). These include water molecules, phytoplankton, colored dissolved organic matter (CDOM; or yellow substance), and detrital particles. In high-wind seas, the OACs may also include bubbles induced by wave breaking, which may increase the backscattering properties significantly [Zhang et al., 1998]. Following Lee et al. [2011],  $R_{rs}(\lambda)$  can be expressed using spectral absorption ( $a$ ) and backscattering ( $b_b$ ) coefficients as

$$R_{rs}(\lambda, \Omega) = \left( G_0^w(\Omega) + G_1^w(\Omega) \frac{b_{bw}(\lambda)}{\kappa(\lambda)} \right) \frac{b_{bw}(\lambda)}{\kappa(\lambda)} + \left( G_0^p(\Omega) + G_1^p(\Omega) \frac{b_{bp}(\lambda)}{\kappa(\lambda)} \right) \frac{b_{bp}(\lambda)}{\kappa(\lambda)}, \quad (6)$$

where the phase-function effects of molecular and particulate scatterings are separated explicitly. In equation (6),  $\kappa = a + b_b$ , while  $\Omega$  represents the solar/viewing geometry. A simplified form has often been used in the literature for low backscattering waters

$$R_{rs}(\lambda) = G \frac{b_{bw}(\lambda) + b_{bp}(\lambda)}{a(\lambda)}, \quad (7)$$

where  $G$  is a model parameter that varies with solar/viewing geometry and scattering phase function and  $b_{bw}$  and  $b_{bp}$  are backscattering coefficients of water molecules (constant) and particles (variable), respectively.

[26] Because  $R_{rs}(670)$  is generally negligible for oligotrophic waters, CI from equation (3) can be approximated as

$$CI \approx G \frac{(2a(443)b_{bw}(555) - a(555)b_{bw}(443)) + (2a(443)b_{bp}(555) - a(555)b_{bp}(443))}{2a(443)a(555)}. \quad (8)$$

ever, its  $R^2$  value is lower than that of the CIA, especially when a linear form is used. Global validation results using this local OCx algorithm showed plateaued performance around  $0.2\text{--}0.3 \text{ mg m}^{-3}$ . More importantly, because it takes a similar band-ratio form, it suffers from the same problems as encountered by the OCx algorithm for low concentrations (see below). Thus, it is listed in Table 2 for demonstration only and was not implemented for MODIS/Aqua or SeaWiFS global data processing.

[24] Because only limited in situ data are available to evaluate algorithm performance at low concentrations (e.g., there is no in situ Chl  $< 0.02 \text{ mg m}^{-3}$ ), below we take a theoretical approach to compare the sensitivity of Chl<sub>CI</sub> and Chl<sub>OC4</sub> algorithms to various perturbations, including sensor noise, atmospheric correction, and noncovarying in-water constituents.

## 6. Algorithm Theoretical Basis and Its Sensitivity to Simulated and Realistic Perturbations

### 6.1. Algorithm Theoretical Basis: Why and When It Works

[25] Assuming that the influence of measurement geometry (i.e., bidirectional reflectance effects) on  $R_{rs}(\lambda)$  can be

[27] Furthermore, because  $b_{bw}(443) \approx 2.6 b_{bw}(555)$  [Morel, 1974] and  $b_{bp}(443) \approx 1.6 b_{bp}(555)$  (assuming a spectral slope of 2), equation (8) can be simplified as

$$CI \approx -G \frac{(a(555) - 0.8a(443))b_{bw}(443) + (a(555) - 1.3a(443))b_{bp}(443)}{2a(443)a(555)} = -G \frac{\Delta_{water} + \Delta_{particles}}{2a(443)a(555)}. \quad (9)$$

**Table 3.** Chl Algorithm Performance From MODIS/Aqua Measurements for Chl  $\leq 0.25 \text{ mg m}^{-3}$ , as Gauged by in Situ Chl<sup>a</sup>

Algorithm	RMS	URMS	Mean Ratio	Median Ratio	MRE	$R^2$ (Linear)	$R^2$ (Log)	$N$
OC3	77.7%	44.2%	1.24	1.05	32.0%	0.42	0.66	63
CI	43.9%	32.7%	1.15	1.04	25.4%	0.62	0.71	63

<sup>a</sup>MODIS/Aqua  $R_{rs}(\lambda)$  were used as the input of all algorithms. URMS, “unbiased” RMS (see text for details); MRE, mean relative error after converting negative errors to positive.

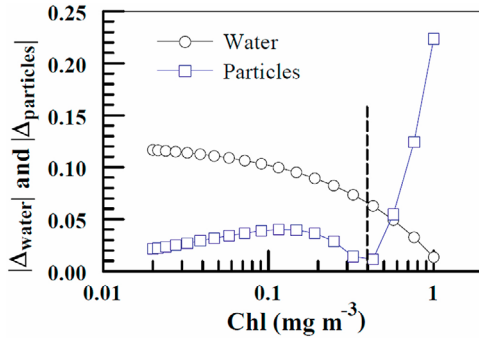


**Figure 6.** Relationship between the two backscattering terms in equation (9) with Chl. To show their relative magnitudes, the absolute values ( $\times 1000$ ) are shown here. Note that for  $\text{Chl} \leq 0.4 \text{ mg m}^{-3}$ , the water term dominates the numerator of equation (9).

[28] Figure 6 shows the two backscattering-related terms ( $|\Delta_{\text{water}}|$  and  $|\Delta_{\text{particles}}|$ ,  $\times 1000$ ) for Chl ranging between 0.02 and  $1.0 \text{ mg m}^{-3}$ , estimated using the Morel and Maritorena [2001] case I model. It shows that for  $\text{Chl} < \sim 0.4 \text{ mg m}^{-3}$ ,  $|\Delta_{\text{water}}|$  overweighs  $|\Delta_{\text{particles}}|$ . This is due to two reasons: (1) low  $b_{\text{bp}}(443)$  relative to  $b_{\text{bw}}(443)$  (e.g., for  $\text{Chl} = 0.1 \text{ mg m}^{-3}$ ,  $b_{\text{bw}}(443) = 0.0025 \text{ m}^{-1}$ ,  $b_{\text{bp}}(443) \sim 0.0015 \text{ m}^{-1}$ ); and (2) when Chl increases, the corresponding increase in  $b_{\text{bp}}(443)$  is compensated by the decrease in  $(a(555) - a(443))$ . These results suggest that for  $\text{Chl} < 0.4 \text{ mg m}^{-3}$ , equation (9) can be further simplified to

$$CI \propto -G \frac{b_{\text{bw}}(443)}{2a(443)}, \quad (10)$$

which is equivalent to the band ratio

$$R = \frac{R_{rs}(443)}{R_{rs}(555)} \approx \frac{b_{\text{bw}}(443) + b_{\text{bp}}(443)}{b_{\text{bw}}(555) + b_{\text{bp}}(555)} \frac{a(555)}{a(443)}. \quad (11)$$

In other words, both CI and  $R$  are inversely related to  $a(443)$ . Because for oligotrophic waters  $a(443)$  is primarily a function of Chl (assuming CDOM covaries with Chl), CI in equation (10) can be expressed as

$$CI \propto -G \frac{b_{\text{bw}}(443)}{2f(\text{Chl})}. \quad (12)$$

[29] This simplified equation, based on several assumptions, explains why Chl can be derived from CI at low concentrations. Below, we use more realistic simulations to demonstrate this concept.

## 6.2. Sensitivity to Perturbations From In-Water Constituents

[30] The empirical Chl algorithms (either OC4 or CIA) are based on the assumption that  $R_{rs}(\lambda)$  is mainly determined by phytoplankton and its direct degradation product (the so-called “Case I” waters [Morel and Prieur, 1977]), or at least other OACs such as CDOM and detrital particles covary with phytoplankton. For low concentrations, both band ratio ( $R$ ) and CI are inversely related to the total absorption

coefficient ( $a(443)$ , equations (10) and (11)), where the contribution of phytoplankton and CDOM/detrital particles to  $a(443)$  must covary in order to derive the former. There has been substantial evidence that the OACs often do not covary even for the open oceans [Loisel et al., 2002; Dierssen, 2010], which may explain why a globally optimized parameterization in OC4 may work well for one ocean basin or one season but its performance can be much worse for another [e.g., Gregg and Casey, 2004]. Thus, for global applications, one measure to assess algorithm robustness is to test its sensitivity to various scenarios where OACs do not covary.

[31] For such a sensitivity analysis, the same approach of Lee et al. [2010] to assess IOP algorithm uncertainty was adapted here for both the OC4 and CIA. Synthetic data ( $R_{rs}(\lambda)$  derived from various IOP combinations) were used to evaluate the impact of IOP variability on Chl retrieval accuracy.

[32] Briefly, starting from equation (6), the geometric parameters ( $G_0^w(\Omega)$ ,  $G_1^w(\Omega)$ ,  $G_0^p(\Omega)$ , and  $G_1^p(\Omega)$ ; in  $\text{sr}^{-1}$ ) were taken as  $(0.0604, 0.0406, 0.0402, 0.1310 \text{ sr}^{-1})$  [Lee et al., 2011]. The absorption and backscattering coefficients were modeled as

$$\begin{aligned} a(\lambda) &= a_w(\lambda) + a_{ph}(\lambda) + a_{dg}(\lambda) \\ b(\lambda) &= b_{bw}(\lambda) + b_{bp}(\lambda), \end{aligned} \quad (13)$$

where  $a_w(\lambda)$  and  $b_{bw}(\lambda)$  are for water molecules and are taken from Pope and Fry [1997] and Morel [1974], respectively. The  $a_{ph}(\lambda)$ ,  $a_{dg}(\lambda)$ , and  $b_{bp}(\lambda)$  are for phytoplankton pigments, detrital particles and CDOM, and particulate matter, respectively, and they are modeled as

$$\begin{aligned} a_{ph}(\lambda) &= a_{ph}(440) a_{ph}^+(\lambda) \\ a_{dg}(\lambda) &= a_{dg}(440) e^{-S(\lambda-440)} \\ b_{bp}(\lambda) &= b_{bp}(440) \left( \frac{440}{\lambda} \right)^\eta. \end{aligned} \quad (14)$$

Here  $a_{ph}^+(\lambda)$  is  $a_{ph}(\lambda)$  normalized to  $a_{ph}(440)$  and is taken from the International Ocean-Colour Coordinating Group (IOCCG) [2006] database. The dependence of  $a_{dg}(\lambda)$  and  $b_{bp}(\lambda)$  on Chl (or  $a_{ph}(440)$ ) was defined as

$$\begin{aligned} a_{dg}(440) &= p_1 a_{ph}(440), \\ b_{bp}(440) &= 0.015 p_2 Chl^{0.62}, \end{aligned} \quad (15)$$

where the exponent of 0.62 was taken from Gordon and Morel [1983] and 0.015 is the backscattering/total-scattering ratio [Sullivan and Twardowski, 2009].

[33] For each Chl value (corresponding to an  $a_{ph}(440)$ ), four parameters can be changed independently in modeling  $R_{rs}(\lambda)$ , and Chl can be retrieved from the modeled  $R_{rs}(\lambda)$  with both OC4 and CIA (equations (2)–(5)) and compared with the input Chl to produce a relative error estimate. These four parameters include  $p_1$ ,  $p_2$ ,  $S$ , and  $\eta$ . Below, we show the results of four scenarios.

### 6.2.1. Scenario 1: Both $a_{dg}$ and $b_{bp}$ Vary Independently From $a_{ph}(440)$

[34] The  $a_{ph}(440)$  was set to be 0.0028, 0.008, 0.012, 0.024, and  $0.05 \text{ m}^{-1}$ , respectively, roughly corresponding to Chl of 0.02, 0.05, 0.1, 0.3, and  $1.0 \text{ mg m}^{-3}$ , respectively [Bricaud et al., 1995]. The minimum  $a_{ph}(440)$  ( $0.0028 \text{ m}^{-1}$ )

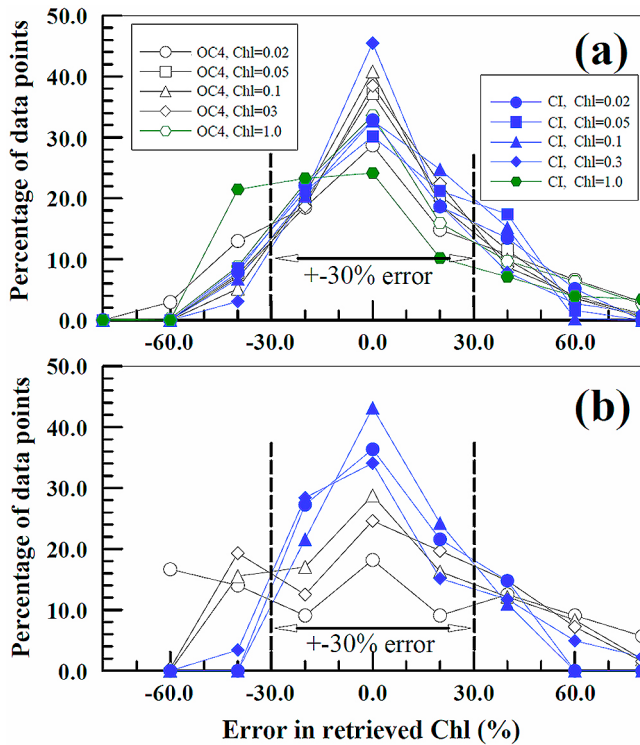


**Figure 7.** Chl algorithm sensitivity to changes of detrital particles and CDOM relative to phytoplankton. (a) Detrital particles and CDOM do not covary, based on 816 model simulations for each Chl value (equations (6) and (13)–(15)). For Chl-relative errors within  $\pm 30\%$  (the two dashed lines), the percentages of data points for Chl = 0.02, 0.05, 0.1, and 0.3 are 62.0% (73.5%), 76.9% (72.5%), 80.3% (77.8%), and 79.5% (85.0%), respectively, for the two algorithms (CIA in the parentheses). Note that the performance of CIA for Chl = 1.0 mg m $^{-3}$  is much worse than OC4. (b) Detrital particles and CDOM covary ( $a_{dg}(440)/b_{bp}(440) = 10.0$ ,  $a_{dg}(440)/a_{ph}(440)$  from 0.3 to 2.0,  $a_{dg}$  slope from 0.013 to 0.019 nm $^{-1}$ ,  $b_{bp}$  slope from 0.5 to 1.5,  $b_{bp}/\text{Chl}$  from 0.1 to 0.6). For Chl-relative errors within  $\pm 30\%$  (the two dashed lines), the percentages of data points for Chl = 0.02, 0.1, and 0.3 are 36.4% (85.2%), 62.1% (89.0%), and 56.8% (77.7%), respectively, for the two algorithms (CIA in the parentheses).

is half of the minimum  $a_{ph}(440)$  in the IOCCG data set and approximates the  $a_{ph}(440)$  values in the South Pacific Gyre [Morel *et al.*, 2007b; Lee *et al.*, 2010]. For each  $a_{ph}(440)$  (and its corresponding Chl),  $p_1$  varied from 0.4 to 2.0 with a step of 0.1 (17  $p_1$  values);  $p_2$  varied from 0.1 to 0.6 with a step of 0.1 (6  $p_2$  values);  $S$  varied from 0.013 to 0.019 with a step of 0.002 (4  $S$  values); and  $\eta$  was set to 0.5 and 1.5. Thus, for each  $a_{ph}(440)$  (Chl), there are 816 sets of  $a$ & $b$ , 816  $R_{rs}$  spectra, and 816 retrieved Chl values. The histogram of the relative errors (relative to the mean results of all retrievals) of the 816 retrieved Chl values from each algorithm is shown in Figure 7a.

[35] Except for the high-concentration case (Chl = 1.0 mg m $^{-3}$ ), the performance of the two algorithms is similar. For Chl-relative errors within  $\pm 30\%$  (Figure 7a, two dashed lines), the percentages of data points for Chl = 0.02, 0.05,

0.1, and 0.3 mg m $^{-3}$  are 62.0% (73.5%), 76.9% (72.5%), 80.3% (77.8%), and 79.5% (85.0%), respectively, for the two algorithms (CIA in parentheses). Furthermore, the CIA yielded less data points than OC4 for errors beyond  $\pm 60\%$ . The percentage numbers for these large errors are 13.5% (5.1%), 4.0% (1.6%), 4.7% (0.2%), and 4.7% (4.1%) for Chl = 0.02, 0.05, 0.1, and 0.3 mg m $^{-3}$ , respectively (CIA in parentheses). Clearly, CIA is comparable to (at least not worse than) OC4 in its sensitivity to Chl-independent IOP perturbations for the applicable range (Chl  $\leq 0.3$  mg m $^{-3}$ ) when all IOPs vary independently.

#### 6.2.2. Scenario 2: Same as Scenario 1, but $a_{dg}$ and $b_{bp}$ Covary

[36] For each Chl (0.02, 0.1, and 0.3 mg m $^{-3}$ ), 264 model simulations were conducted, where  $a_{dg}$  slope varied from 0.013 to 0.019 nm $^{-1}$  (step of 0.002),  $b_{bp}$  slope varied from 0.5 to 1.5 (step of 0.2),  $b_{bp}/\text{Chl}$  varied from 0.1 to 0.6 (step of 0.05), and  $a_{dg}(440)/b_{bp}(440)$  was forced to be 10 (i.e., they covaried). In these simulations  $a_{dg}(440)/a_{ph}(440)$  ranged between 0.3 and 2.0, consistent with those found from most natural waters. The sensitivities of the OC4 and CIA algorithms to these IOP changes are presented in Figure 7b. For Chl-relative errors within  $\pm 30\%$  (Figure 7b, two dashed lines), the percentages of data points for Chl = 0.02, 0.1, and 0.3 are 36.4% (85.2%), 62.1% (89.0%), and 56.8% (77.7%), respectively, for the two algorithms (CIA in parentheses). Clearly, for low concentrations (Chl  $\leq 0.3$  mg m $^{-3}$ ), the CIA is less sensitive than OC4 to independent IOP perturbations when  $a_{dg}$  and  $b_{bp}$  covary.

#### 6.2.3. Scenario 3: $a_{dg}$ Varies Independently From $a_{ph}(440)$ but $b_{bp}$ Covaries With $a_{ph}(440)$

[37] For each  $a_{ph}(440)$ ,  $p_2$  was set to 0.45,  $\eta = 1.0$ ,  $S = 0.016$ , but  $p_1$  was changed from 0.3 to 2.5 with a step of 0.1 (23  $p_1$  values). Figure 8a shows that the relative errors in the retrieved Chl from both algorithms change from negative to positive with increasing  $a_{dg}/a_{ph}$  ratios, an expected result where the increased CDOM or detrital particles were mistakenly regarded as Chl because they all strongly absorb the blue light. For extremely low concentrations (Chl < 0.1), errors from the CIA are slightly higher, but for higher concentrations, the errors approach those from the OC4 algorithm. For the entire simulation range, the mean relative errors (after converting negative to positive values) for Chl = 0.02, 0.05, 0.1, and 0.3 mg m $^{-3}$  are 30.4% (30.6%), 23.2% (30.3%), 23.4% (28.3%), and 22.5 (23.1%), respectively (CIA in parentheses). For the extreme case of Chl = 1.0 mg m $^{-3}$ , errors from the CIA are lower than those from the OC4 algorithm, especially when  $a_{dg}(440)/a_{ph}(440)$  is  $> 2.0$  or  $< 1.0$ . In general, for Chl  $\leq 0.25$  mg m $^{-3}$  and the moderate range of  $a_{dg}(440)/a_{ph}(440)$  (1.0–2.0), the retrieval errors from the two algorithms are similar.

#### 6.2.4. Scenario 4: $b_{bp}$ Varies Independently From $a_{ph}(440)$ but $a_{dg}$ Covaries With $a_{ph}(440)$

[38] For each  $a_{ph}(440)$ ,  $p_1$  was set to 1.0,  $\eta = 1.0$ ,  $S = 0.016$ , but  $p_2$  was changed from 0.1 to 0.6 with a step of 0.05 (11  $p_2$  values). Figure 8b shows that for Chl < 0.3 mg m $^{-3}$ , the CIA yielded much lower relative errors for all cases regardless of the error sign. For the entire simulation range, the mean relative errors (after converting negative to positive values) for Chl = 0.02, 0.05, 0.1, and 0.3 mg m $^{-3}$  are 17.4% (9.0%), 11.6% (6.9%), 11.1% (4.8%), and 11.2% (4.3%), respectively (CIA in parentheses). The errors from the CIA

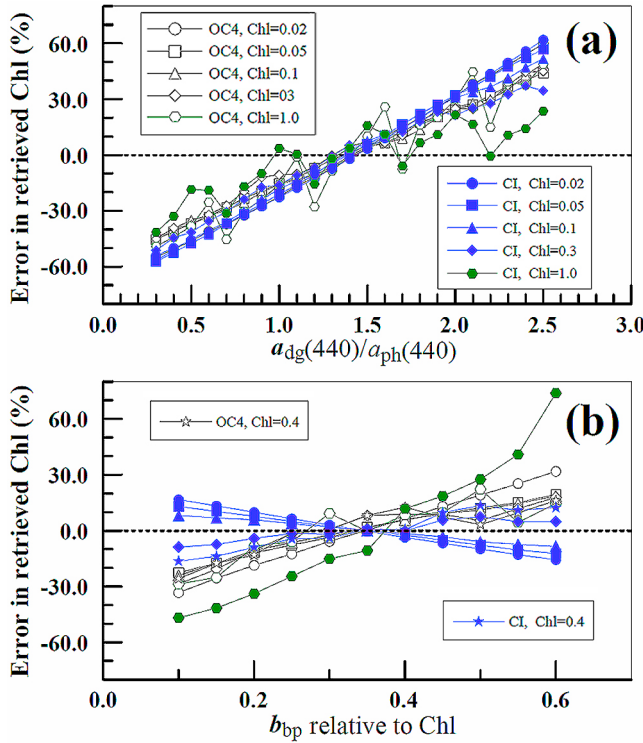


**Figure 8.** Chl algorithm sensitivity to (a) independent changes of absorption of detrital particles and CDOM ( $a_{dg}$ ) relative to Chl and (b) independent changes of particular backscattering ( $b_{bp}$ ) relative to Chl, based on model simulations for each Chl value (equations (6) and (13)–(15)). Note that in Figure 8b, the added simulation was for Chl = 0.4 (stars), when the errors in the CI retrievals are shown to approach those of the OC4 retrievals. In Figure 8a, for the entire simulation ranges, the mean relative errors (after converting negative to positive values) for Chl = 0.02, 0.05, 0.1, and 0.3 mg m<sup>-3</sup> are 30.4% (30.6%), 23.2% (30.3%), 23.4% (28.3%), and 22.5 (23.1%), respectively (CIA in the parentheses). In Figure 8b, the mean relative errors are 17.4% (9.0%), 11.6% (6.9%), 11.1% (4.8%), and 11.2% (4.3%), respectively. Note that the performance of CI for Chl = 1.0 mg m<sup>-3</sup> is much worse than OC4.

change sign between 0.1 and 0.3 mg m<sup>-3</sup>. At Chl = 0.4 mg m<sup>-3</sup>, the CIA errors approach those from the OC4. At Chl = 1.0 mg m<sup>-3</sup>, errors from the CIA are significantly higher than those from the OC4. These results suggest that for Chl < 0.4 mg m<sup>-3</sup>, the performance of the CIA is often significantly better than the OC4 when  $b_{bp}$  varies independently from  $a_{ph}(440)$  (or Chl). The negative slope in Figure 8b for the CIA with Chl  $\leq 0.1$  mg m<sup>-3</sup> (i.e., errors change from positive to negative with increasing  $b_{bp}/\text{Chl}$ ) has significant implications for oligotrophic waters. For example, with increasing detrital particles, the increased detrital absorption will lead to overestimates in Chl<sub>CI</sub> (Figure 8a), while the increased backscattering will lead to underestimates in Chl<sub>CI</sub> (Figure 8b). Thus, these two effects will be partially compensated for low concentrations when  $a_{dg}$  and  $b_{bp}$  covary (Figure 7b).

[39] The results above are based on simulated data sets, some of which may not be realistic in nature. Indeed, on

large dynamic scales, the absorption IOPs often covary [Morel, 2009], although their relative proportions in modulating the  $R_{rs}(\lambda)$  may change from one ocean basin to another. For example, although the ratio of  $a_{dg}(440)/a_{ph}(440)$  showed a weak seasonality in an oligotrophic ocean site and there was an observable temporal lag between the two absorption terms, they did show high correlations in the temporal patterns [Hu et al., 2006]. In contrast to absorption OACs,  $b_{bp}$  relative to Chl may vary substantially in both space and time [Loisel et al., 2002; Dierssen, 2010], where the CIA should perform significantly better than the OC4 algorithm in the algorithm tolerance to independent  $b_{bp}$  changes for low-concentration waters.

[40] Overall, from these model-based simulations, we believe that with error-free  $R_{rs}(\lambda)$  as the input, the CIA should perform at least equivalently to the OC4 algorithm for Chl  $\leq 0.3$  mg m<sup>-3</sup>, if not better. These results are also consistent with those shown in Figure 3, when in situ data (assumed error free, but they certainly contained both measurement and data reduction errors) were used to evaluate algorithm performance, and with those shown in Figure 6.

### 6.3. Sensitivity to Digitization Noise and Atmospheric Correction Errors

[41] The above simulations are based on the assumption that the inputs of the algorithms, namely, the  $R_{rs}(\lambda)$  data, are error free. In practice,  $R_{rs}(\lambda)$  derived from satellite measurements may contain various errors from imperfect radiometric calibration, instrument noise and digitization round-off noise, imperfect atmospheric correction, residual errors from whitecap and sun glint corrections, and stray light contaminations (equation (1) and Figure 1).

[42] Assuming an error-free calibration and an error-free atmospheric correction scheme, Hu et al. [2001] used model simulations to evaluate the SeaWiFS data product uncertainties originating from instrument and digitization noise alone. They found that (1) errors in the retrieved  $R_{rs}(\lambda)$  and band-ratio Chl were primarily from noise-induced perturbations in the atmospheric correction, which were propagated and enlarged from the near-IR bands to the visible bands, and (2) relative errors in the band-ratio Chl were more prominent in both low (<0.1 mg m<sup>-3</sup>) and high (>10 mg m<sup>-3</sup>) Chl ranges than in the intermediate Chl ranges.

[43] The same simulations were applied here to compare relative errors in Chl<sub>OC4</sub> and Chl<sub>CI</sub> due to digitization/noise. Briefly, random noise at the level between  $-0.5\delta(\lambda)$  and  $0.5\delta(\lambda)$  was added to  $\rho_t(\lambda)$  in equation (1), where  $\delta(\lambda)$  is the spectral remote-sensing reflectance corresponding to one digital count in the individual band

$$\rho'_t(\lambda) = \rho_t(\lambda) + \text{noise}. \quad (16)$$

$\rho_t(\lambda)$  and  $\rho'_t(\lambda)$  were fed to the identical atmospheric correction and bio-optical inversion algorithms under various observation conditions (aerosol type and optical thickness, solar/viewing geometry), the derived Chl from the noise-free  $\rho_t(\lambda)$  and noise-added  $\rho'_t(\lambda)$  were compared, and relative error was assessed. Figures 9 and 10 show examples of the simulation results. For 10,000 model runs of the given aerosol information (maritime aerosol with relative humidity of 90%) and solar/viewing geometry (scene center, solar zenith angle  $\theta_o = 60^\circ$ ), the errors in the retrieved  $R_{rs}(\lambda)$  due

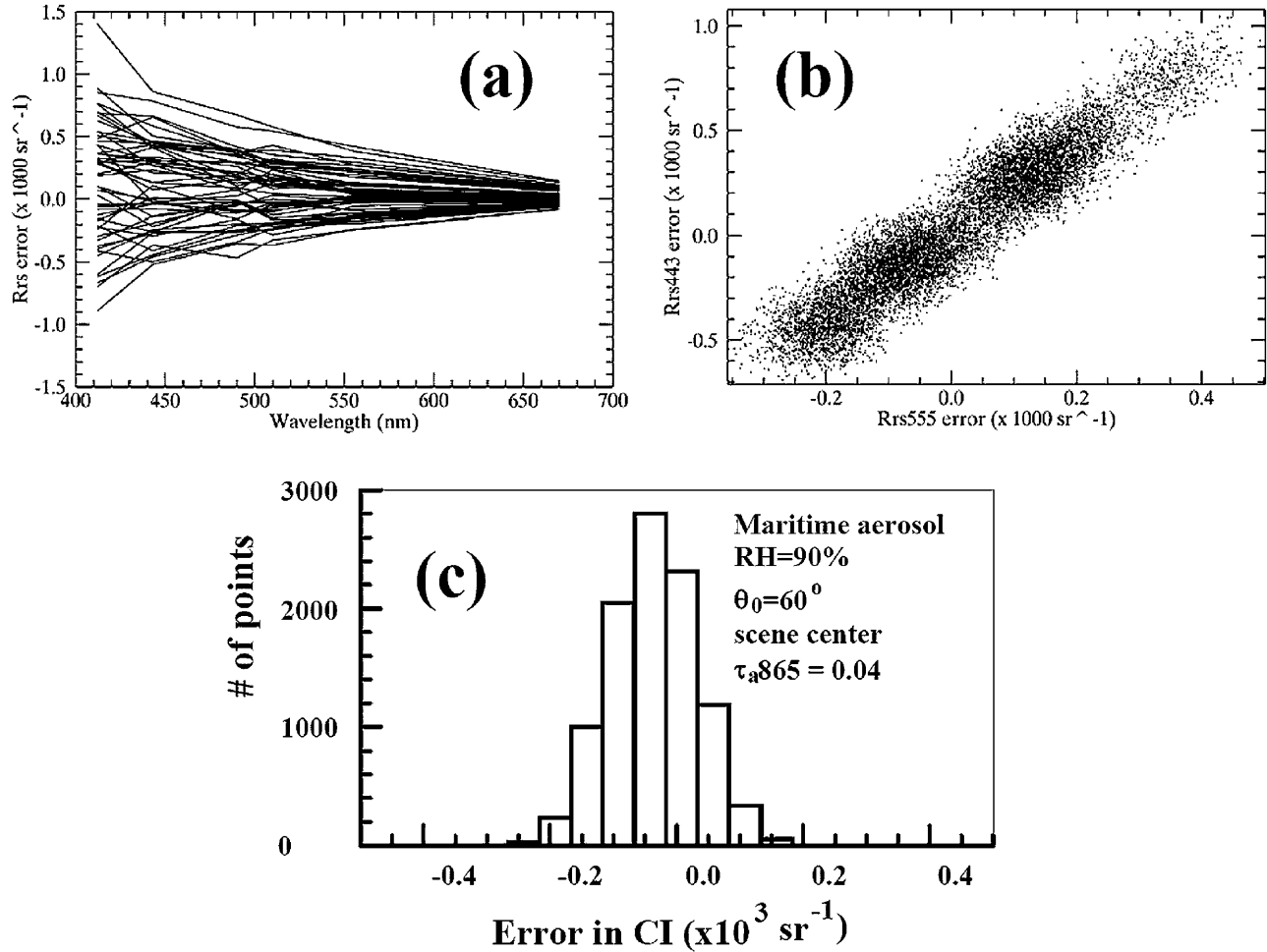


**Figure 9.** Errors in  $R_{rs}(\lambda)$  and CI induced by SeaWiFS digitization noise after applying the *Gordon and Wang* [1994a] atmospheric correction. Most of the errors are due to the impact of the small noise on the atmospheric correction bands in the near infrared, which extrapolate the atmospheric properties to the visible [Hu et al., 2001]. (a and b) These errors are approximately linear to changing wavelengths and can thus be corrected to first order by the CI algorithm (equation (3) and Figure 2), resulting in smaller errors in CI (and  $\text{Chl}_{\text{CI}}$ ; Figure 10). (c) Errors in the retrieved CI, with model parameters annotated. Results from other modeling scenarios are different, but the principles in reducing the noise-reduced errors using the CI are the same.

to digitization round-off and instrument noise alone are presented in Figure 9. To first order, the errors are spectrally linear (Figure 9a), and errors at 443 nm are roughly twice those at 555 nm (Figure 9b). Because of the approximate linearity, most of these errors were canceled in equation (3), resulting in much smaller errors in the CI (Figure 9c). In contrast, these same  $R_{rs}(\lambda)$  errors can only be canceled to a lesser degree in the band-ratio  $R$  (equation (2)), especially when the ratio is significantly different from 2 (when the ratio is  $\sim 2$ , adding twice as much error in the numerator as in the denominator will make the ratio unchanged). For the oligotrophic oceans,  $R_{rs}(555)$  is small (the blue/green ratio  $R$  may reach 8.0), then large errors in the blue/green ratio could be resulted when  $R_{rs}(\lambda)$  contains small, spectrally linear perturbations. Thus, the different sensitivity of  $R$  and CI to the digitization noise-induced errors leads to different accuracy in the retrieved Chl (Figure 10). For the Chl range considered here, while the relative errors in  $\text{Chl}_{\text{OC4}}$  increased

sharply with decreasing Chl, the errors in  $\text{Chl}_{\text{CI}}$  remained unchanged at a much lower level. Simulation results for other aerosol and solar/viewing geometry were different from those shown in Figures 9 and 10, but the general pattern remained the same, i.e., relative errors in  $\text{Chl}_{\text{OC4}}$  were always higher than in  $\text{Chl}_{\text{CI}}$  for  $\text{Chl} < 0.4 \text{ mg m}^{-3}$ , with only the former varying with Chl.

[44] Clearly, for  $\text{Chl} < 0.4 \text{ mg m}^{-3}$ ,  $\text{Chl}_{\text{CI}}$  is much less sensitive than  $\text{Chl}_{\text{OC4}}$  to digitization noise-induced errors for SeaWiFS. In practice, the atmospheric correction scheme implemented in SeaDAS has inherent errors to within  $\pm 0.002$  in reflectance at 443 nm ( $\rho_{\text{W}443}$ ), which is the basis for the 5% fidelity in the retrieved reflectance at 443 nm for clear waters [Gordon and Wang, 1994a; Gordon, 1997]. The  $\pm 0.002$  reflectance errors are equivalent to  $R_{rs}(443)$  errors of approximately  $\pm 0.002/\pi = \pm 0.0006 \text{ sr}^{-1}$ , corresponding to  $R_{rs}(555)$  errors of about  $\pm 0.0003 \text{ sr}^{-1}$ . These additional errors are comparable to those due to SeaWiFS digitization

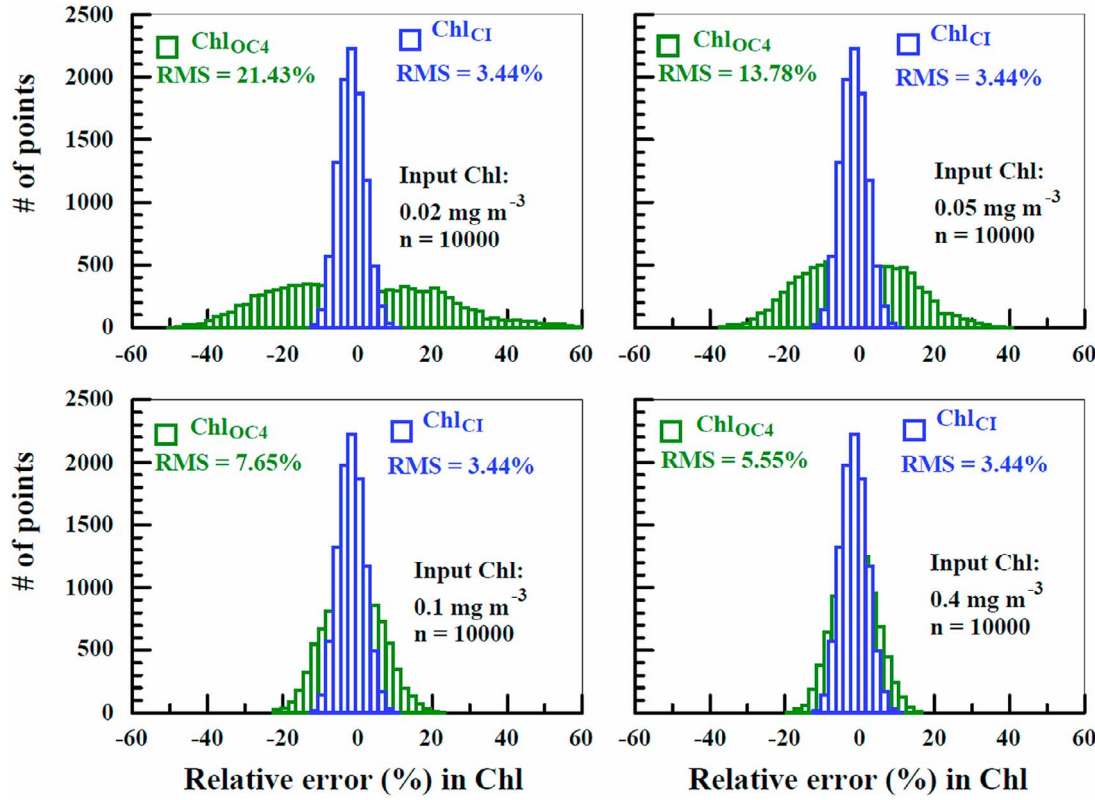


**Figure 10.** Error distribution in the retrieved Chl due to digitization round-off and instrument noise-induced  $R_{rs}(\lambda)$  errors for a clear maritime atmosphere (see Figure 9). In situ  $R_{rs}$  data for the input Chl concentrations (from  $0.02$  to  $0.4\text{ mg m}^{-3}$ ) were combined with the  $R_{rs}(\lambda)$  errors to estimate Chl, where the “true” Chl was determined from the input  $R_{rs}$  data free of errors. The differences were used to determine the relative retrieval errors. Note that the CI-based retrieval errors are independent of Chl concentrations.

noise (Figures 9a and 9b) and are independent of instrument sensitivity (i.e., they apply to all ocean color sensors including SeaWiFS and MODIS/Aqua). Figure 11 shows that Chl<sub>CI</sub> is nearly immune to such residual errors resulting from atmospheric correction because they are spectrally related. Even when the atmospheric correction error is 3 times the mission specification, relative errors in the retrieved Chl<sub>CI</sub> for the entire Chl range are still  $<2.0\%$  for most aerosol types (Figure 11b;  $\alpha = 0.7$ ). In comparison, relative errors in the retrieved Chl<sub>OC4</sub> are 10 times higher for Chl  $< 0.1\text{ mg m}^{-3}$ . Furthermore, while the digitization noise-induced errors, assumed randomly distributed, may be averaged out if a sufficient number of points (image pixels) are available, the atmospheric correction errors may create a bias at various spatial and temporal scales because the conditions that result in these atmospheric correction errors may not be random (yet the spatial and temporal distributions of these conditions are unknown). This effect will be shown below with satellite data analysis.

## 7. Evaluation Using SeaWiFS and MODIS/Aqua Imagery

[45] The CIA was applied to SeaWiFS Level-2 GAC data to derive Chl<sub>CI</sub> and compared with the default Chl<sub>OC4</sub>. In the comparison, the following quality control flags were used to discard all suspicious data points: atmospheric correction failure (bit 1), land (bit 2), high sun glint (bit 4), total

radiance greater than knee (a predefined threshold, bit 5), large satellite zenith (bit 6), stray light (bit 9), cloud/ice (bit 10), coccolithophores (bit 11), large solar zenith (bit 13), low water-leaving radiance (bit 15), chlorophyll algorithm failure (bit 16), questionable navigation (bit 17), near-IR exceeds maximum iteration (bit 20), chlorophyll warning (bit 22), and atmospheric correction warning (bit 23). These are the same flags as used to perform data quality control during SeaWiFS and MODIS Level-3 data binning. Figure 1 shows the images of Chl<sub>OC4</sub>, Chl<sub>CI</sub>,  $\tau_{865}$ , and  $R_{rs}(555)$  for the North Atlantic Ocean Gyre from an arbitrarily selected date.

[46] The image speckling effect is apparent in the Chl<sub>OC4</sub> image (Figure 1a), where discontinuity and patchiness can also be found (a few examples are outlined in circles). While the speckling effect (pixelization noise) is due primarily to digitization noise-induced errors, the patchiness is more likely due to atmospheric correction errors and other correction errors (such as whitecap correction). Indeed, similar discontinuity and patchiness are also found in the  $\tau_{865}$  and  $R_{rs}(555)$  images (Figures 1c and 1d). Such sharp changes and patchiness in both the atmosphere and ocean properties in an ocean gyre are unlikely to be realistic but can only be due to algorithm errors. These errors occasionally led to  $R_{rs}(555)$  values less than the theoretical limit for even the clearest ocean waters,  $0.001\text{ sr}^{-1}$ . In contrast to the Chl<sub>OC4</sub> image that contains speckling noise and patchiness, the

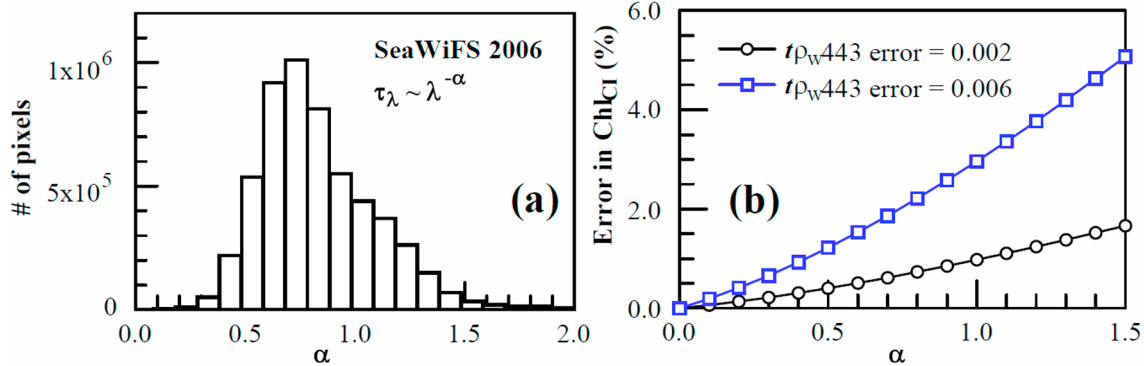


**Figure 11.** Sensitivity of Chl<sub>CI</sub> to atmospheric correction errors. (a) SeaWiFS global data during 2006 showed aerosol-type (defined as the aerosol scattering angstrom exponent,  $\alpha$ ) distributions. More than 99% of  $\alpha$  falls between 0.0 and 1.5. (b) Errors in the retrieved Chl<sub>CI</sub> for two atmospheric correction errors ( $t_{p_w}443 = 0.002$  and  $0.006$ ) for various  $\alpha$  values. The  $t_{p_w}443$  error =  $\pm 0.002$  is the ocean color satellite mission specification, corresponding to about 5%  $R_{rs}443$  error for blue waters. The  $t_{p_w}443$  error = 0.006 artificially increased this threshold to 3 times higher, leading to a relative  $R_{rs}555$  error approaching 100% for  $\alpha = 0.7$ . Even under this extreme condition, the corresponding Chl<sub>CI</sub> retrieval error is still <2.0%. Note that similar to those shown in Figure 10, the percentage Chl<sub>CI</sub> errors are independent of Chl values.

Chl<sub>CI</sub> image in Figure 1b, derived from identical  $R_{rs}(\lambda)$  data as used to derive Chl<sub>OC4</sub>, shows much smoother and more spatially coherent distributions even near cloud edges. These results strongly suggest that Chl<sub>CI</sub> is much more immune to both digitization noise and atmospheric correction errors, consistent with those found from the simulations (Figures 9–11). Note that some of the noises are due to stray light contamination near clouds, but most of these noises are effectively removed by the CIA, suggesting that these noises are also spectrally linear.

[47] To quantify the image speckling noise from the satellite images, a  $3 \times 3$  median filter was used to smooth the Chl images, with the result assumed as the truth. The relative difference between the original data and the smoothed data was assumed to be primarily from digitization noise-induced errors. To avoid potential assessment bias due to insufficient sample size, all valid SeaWiFS Level-2 pixels for the  $20^\circ \times 20^\circ$  box in the North Atlantic Gyre from the 599 images in 1998 were queried, and RMS error for each predefined Chl interval was calculated. Figure 12a shows that the RMS errors in Chl<sub>OC4</sub> increase sharply with decreasing Chl, while these errors in Chl<sub>CI</sub> remain stable at a much lower level. The overall patterns agree very well with those from the model simulations (Figure 10), suggesting that most of these speckling errors originated from digitization noise (through error propagation in the atmospheric correction). The discrepancy in the error magnitude between Figure 10 and Figure 12a originated from the different scenarios: Figure 10 is for a single observing condition based on simulations, while Figure 12a accounts for all observing conditions for the entire year. Another reason may be due to stray light and imperfect sun glint and whitecap corrections, which were not accounted for in the simulations. Indeed, the SeaWiFS GAC data were collected by resampling the 1 km data every fourth row and column, and the potential small clouds between the resampled pixels may lead to stray light contamination to the valid pixels. These potential stray light problems for SeaWiFS GAC data cannot

be assessed from the data alone because of the data gap (i.e., the resampled “1 km” pixels in the GAC data are 3 km away from each other). Yet, Figures 12a and 1 show that under realistic measurement conditions, the relative RMS errors in Chl<sub>CI</sub> are significantly smaller than in Chl<sub>OC4</sub> for low concentrations. This finding holds true even when the SeaWiFS local area coverage (LAC) data at 1 km resolution are used for the same comparison. Similar findings were obtained for MODIS/Aqua 1 km resolution data (Figure 12b).

[48] The statistics in Figure 12a also suggest the improvement of the CI algorithm in reducing the number of extreme data points from the OC4 algorithm (e.g., Chl <  $0.02 \text{ mg m}^{-3}$ ). These extreme points are not only due to digitization noise-induced errors but also due to atmospheric correction errors or other algorithm artifacts (whitecap and sun glint corrections, stray light contamination), or both. Indeed, the changes in the number of valid pixels for each Chl interval from Chl<sub>OC4</sub> to Chl<sub>CI</sub> suggest data redistribution, which will affect time series analysis over low-concentration waters. Similar observations were found from MODIS/Aqua data (Figure 12b).

[49] SeaWiFS data for the North Atlantic and South Pacific Gyres for an entire year were visualized to examine whether the above observations could be generalized. The results confirmed those shown in Figure 1 and suggest that most digitization noise-related speckling errors can be removed using the CIA for low concentrations, and many other algorithm artifacts (sun glint and whitecap corrections, atmospheric correction, and stray light contamination) can also be reduced with the CIA. The effect of such correction on time series analysis is demonstrated below.

## 8. Comparison Between Chl<sub>OC4</sub> and Chl<sub>CI</sub> Time Series

[50] Figure 13 shows a 1 year time series at an oligotrophic site in the North Atlantic Gyre using SeaWiFS daily Level-2 GAC data. While the Chl<sub>OC4</sub> data show high

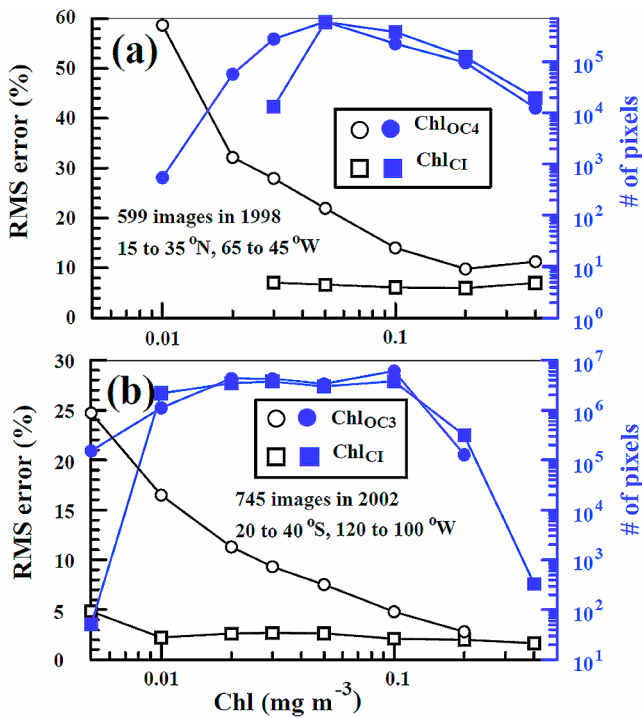


**Figure 12.** Chl errors resulted from digitization round-off and instrument noise, obtained from SeaWiFS and MODIS/Aqua image analyses. (a) Statistics of speckling error in SeaWiFS GAC images in 1998 ( $n = 599$ ) for a  $20^\circ \times 20^\circ$  region in the Sargasso Sea. The speckling error is defined as the relative difference between the original Level-2 Chl and a  $3 \times 3$  median-filter smoothed Level-2 Chl, with the assumption that most noise-induced speckling errors are removed in the latter. Note that while the RMS errors in Chl<sub>OC4</sub> increase sharply with decreasing concentrations, RMS errors in Chl<sub>CI</sub> remain stable at a much lower level in the entire concentration range here. The overall patterns agree well with those from the model simulations (Figure 10), suggesting that most of these speckling errors originate from digitization round-off and instrument noise (through atmospheric correction). The total number of valid pixels from each algorithm indicates that all Chl<sub>OC4</sub>  $\leq 0.02 \text{ mg m}^{-3}$  appear unrealistic due to primarily atmospheric correction artifacts. (b) Same as in Figure 12a, but data were extracted from MODIS/Aqua Level-2 images in 2002 ( $n = 745$ ) for a  $20^\circ \times 20^\circ$  subregion in the Southern Pacific.

speckling (high standard deviations at each  $3 \times 3$  point) and nearly no seasonality due to other errors, the Chl<sub>CI</sub> data show much cleaner time series and also a clear seasonality. Note that the standard deviation at each point represents digitization noise-induced errors, but the deviation of the  $3 \times 3$  mean data value (e.g., those outlined in circles in Figure 13) from the seasonal pattern represents errors from other sources such as imperfect atmospheric correction, which are effectively removed in the Chl<sub>CI</sub> time series. This effect also remains for the monthly composite time series at the same location (Figure 14). The seasonality of Chl<sub>CI</sub> is clear in every year of the 13 year time series (note that there were some missing data after 2005 due to instrument operations) but less apparent in the corresponding Chl<sub>OC4</sub> time series.

The mean monthly variance (standard deviation over mean) was reduced from 26.6% in Chl<sub>OC4</sub> to 9.9% in Chl<sub>CI</sub>. All these results suggest improvements of the CIA in constructing Chl time series for oligotrophic waters.

[51] The improvement of Chl<sub>CI</sub> in deriving a better time series is primarily because of reduction of algorithm-induced errors as opposed to the reduction in speckling noise. As shown in Figures 1 and 13, as well as in the study by *Hu et al. [2001]*, while the image speckling noise can be removed using pixel averaging (either  $3 \times 3$  or temporal averaging), algorithm-induced errors cannot be removed this way and will ultimately propagate to higher-level data products in global or regional time series analyses. Thus, the significantly reduced errors in the Chl<sub>CI</sub> data product may result in more consistent spatial and temporal patterns than the current OCx algorithm for the oligotrophic oceans.

## 9. Discussion

### 9.1. Algorithm Accuracy: Band Ratio or Band Difference?

[52] The comprehensive analyses above, from direct validation, theoretical background, and sensitivity analysis through bio-optical and atmospheric correction simulations to satellite data product comparison, all suggest that the CIA is more robust than the OC4 (or OCx) algorithm for low concentrations ( $\text{Chl} \leq 0.25 \text{ mg m}^{-3}$ ). This range corresponds to about 78% of the global ocean area, suggesting potentially profound effects in global- and regional-scale studies. In particular, studies focusing on ocean gyre variability [*McClain et al., 2004b; Polovina et al., 2008*] and second-order ocean chlorophyll variability [*Brown et al., 2008*] may need to be revisited with the data products generated with the new algorithm.

[53] The improved performance of the CIA for low concentrations ( $\text{Chl} \leq 0.25 \text{ mg m}^{-3}$ ) is primarily due to two reasons. First, for most cases considered, it appears equivalent and often more tolerant (i.e., less sensitive) than the OCx algorithm to in-water perturbations when the various OACs (especially particle backscattering) do not covary. Although the noncovariance of the OACs may represent a primary reason why a global algorithm may not work for a particular region [*Claustre and Maritorena, 2003; Dierssen, 2010*], it is not the objective of any empirical algorithm to solve this global puzzle. Likewise, the chlorophyll-specific absorption coefficient (i.e., absorption per Chl) may also vary substantially due to different pigment composition and phytoplankton size, but all global empirical algorithms would suffer the same from this variability. At the least, the CIA is equivalent or slightly better for most oligotrophic waters than the OCx algorithm to the in-water perturbations. The improved performance over backscattering perturbations is of particular importance, as this may lead to an improved Chl retrieval in scattering-rich low-concentration waters due to bubbles or other marine organisms such as coccolithophores. Second and most importantly, the CIA can partially remove most algorithm artifacts induced by digitization-noise errors, atmospheric correction errors, residual errors due to imperfect sun glint and whitecap corrections, and some of the stray light contamination. Although the band-ratio algorithm can also remove some of

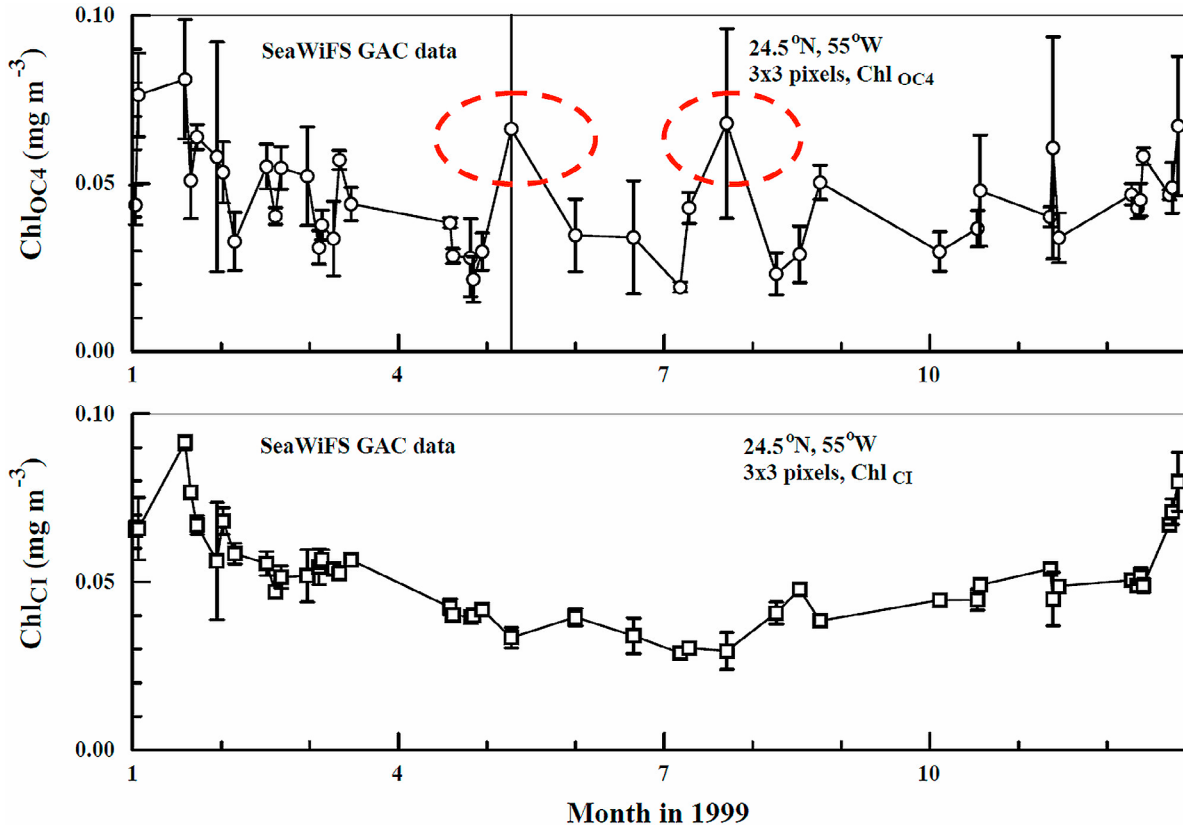


**Figure 13.** Chl (in  $\text{mg m}^{-3}$ ) time series derived from SeaWiFS GAC  $R_{rs}(\lambda)$  data using the (top) OC4v6 algorithm and the (bottom) CI algorithm. Data were extracted from  $3 \times 3$  pixels centered at  $24.5^\circ\text{N}, 55^\circ\text{W}$  from the daily measurements. For any given image (date), only when more than half of the pixels (in this case,  $\geq 5$  pixels) contained valid data (i.e., not associated with any suspicious flags) were statistics estimated. While the magnitudes of the standard deviations (vertical bars) indicate speckling errors caused by digitization round-off and instrument noise (Figures 9, 10, and 12), deviations from the general seasonal pattern (e.g., outlined in the dashed circles) are from atmospheric correction errors (Figure 11). Both errors are significantly reduced in Chl<sub>CI</sub>.

these errors to a certain degree, the removal is much less effective for low-concentration waters.

[54] Indeed, the concept to use alternative ways instead of band-ratio algorithms to derive Chl is not new. *Campbell and Esaias* [1983] proved why a curvature algorithm in the form of  $S_j^2/(S_i S_k)$  could be used to derive chlorophyll concentrations. Here  $S_j$  represents the measured signal in one band (calibrated or not) and  $S_i$  and  $S_k$  represent the signals from the two neighboring bands. *Barnard et al.* [1999] showed the validity of a similar curvature approach to derive absorption coefficients. *Lee and Carder* [2000] further used simulations to compare band-ratio and band-curvature algorithm performance and highlighted that band-ratio algorithms were more sensitive to a wider dynamic range. More recently, a spectral curvature between 443 and 555 nm was used to classify *Karenia brevis* (a toxic dinoflagellate) blooms from other blooms in the Gulf of Mexico [Tomlinson et al., 2009], yet no attempt was made to relate the curvature to Chl.

[55] Early pioneer efforts for algorithm development also proposed band-difference algorithms [*Viollier et al.*, 1978; *Viollier et al.*, 1980; *Tassan*, 1981], where the difference between two neighboring blue and green bands was related

to surface Chl. The rationale for choosing a blue-green band difference was because of its tolerance to various errors in the spectral reflectance, including whitecaps [Tassan, 1981]. However, through model estimates, *Gordon and Morel* [1983] argued that because reflectance is, in principle, proportional to backscattering to the first order (i.e.,  $R_{rs} \propto b_b/a$ ; see equation (7)), a band-difference algorithm will retain most variability of  $b_b$  relative to phytoplankton, thus subject to large errors if  $b_b$  varies independently from phytoplankton (e.g., sediment-rich coastal waters). In contrast, as long as the spectral variability of  $b_b$  is within a narrow range, a band-ratio algorithm will overcome such variability to first order, making the algorithm less sensitive to independent  $b_b$  changes. For this reason, except for a handful of studies in the 1980s, band-difference algorithms have rarely been used in the published literature. One exception was perhaps the normalized difference pigment index (NDPI) algorithm proposed by *Frouin* [1997] for the POLDER instrument [*Mukai et al.*, 2000], which combined the band-difference and band-ratio forms using the 443, 490, and 555 nm bands. The NDPI algorithm is essentially a band-ratio algorithm, although the 443–555 difference in the numerator has been shown to remove some noise. A similar combination of band

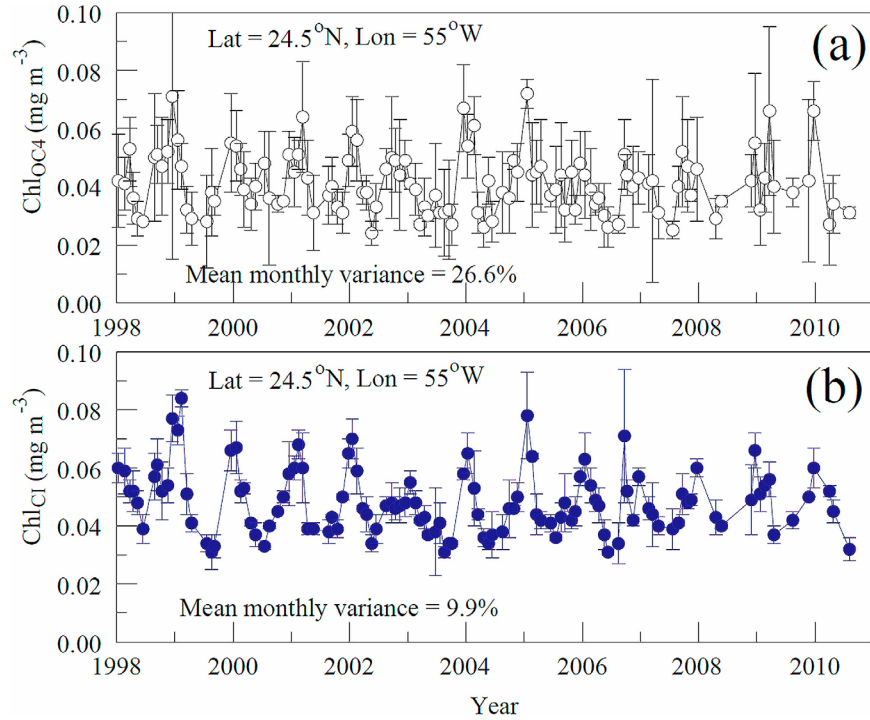


**Figure 14.** Chl (in  $\text{mg m}^{-3}$ ) time series derived from SeaWiFS GAC  $R_{rs}(\lambda)$  data using (a) the OC4v6 algorithm and (b) the CI algorithm. Data were first extracted from  $3 \times 3$  pixels centered at  $24.5^\circ\text{N}$ ,  $55^\circ\text{W}$  from the daily measurements. For any given image (date), only when more than half of the pixels (in this case,  $\geq 5$  pixels) contained valid data (i.e., not associated with any suspicious flags) were statistics estimated. The daily data were then averaged for the calendar month to construct the monthly time series. Note that SeaWiFS was not continuously operational after 2005 because of instrument operations. Note the significant reduction of monthly variance from ChlOC4 to ChlCI because the latter is more tolerant to both digitization noise and atmospheric correction errors.

difference and band ratio was proposed for the recently launched Geostationary Ocean Color Imager (GOCI), yet its performance over oligotrophic waters needs to be validated. Note that because most of the atmospheric correction residual errors are not spectrally flat (Figure 11a), most of the residual errors are retained in the 443–555 (or other blue-green) difference algorithms, yet they can be successfully removed by the CIA because of the three-band design (Figure 11b).

[56] The fundamental principles and model simulation results in sections 6.1 and 6.2 suggest that the arguments by *Gordon and Morel* [1983], made for moderate to high-concentration waters, on the weakness of band-difference algorithms should be revisited for oligotrophic oceans. Indeed, for  $\text{Chl} \leq 0.3 \text{ mg m}^{-3}$ , the simulation results showed that a three-band difference algorithm (i.e., the CIA) is more tolerant to independent  $b_b$  changes than the band-ratio algorithm. This may appear against intuition for the reasons outlined by *Gordon and Morel* [1983]. However, equation (6) shows that  $R_{rs}(\lambda)$  is not proportional to particulate backscattering ( $b_{bp}$ ) but influenced by both molecular and particle backscattering ( $b_{bw}$  and  $b_{bp}$ ). When Chl is low, the proportion of  $b_{bp}$  to total  $b_b$  is relatively small (e.g.,  $b_{bp}(440) \sim 35\%$  of total  $b_b(440)$  for  $\text{Chl} = 0.1 \text{ mg m}^{-3}$ , and the other 65% is due to a constant water molecular scattering), resulting in the tolerance of the CIA to independent  $b_{bp}$

changes. In addition, the design of CI (equation (3)) places more relative weighting of  $b_{bw}$  than for  $b_{bp}$  for low concentrations. For high-Chl waters (e.g., Chl =  $1.0 \text{ mg m}^{-3}$ ; Figure 8b),  $b_{bp}$  dominates  $b_b$ , and the CIA becomes more sensitive than the OC4 algorithm to independent  $b_{bp}$  changes, consistent with the arguments of *Gordon and Morel* [1983]. For the tolerance to other errors (sensor noise, atmospheric correction residual errors, sun glint and white-cap correction residual errors, stray light contamination, etc.), the CIA is much better than the band-ratio algorithm, confirming Tassan's argument. The CIA, however, is not a simple blue-green difference but takes a third band in the red to account for the various errors listed above.

[57] The stability of empirical Chl algorithms to independent  $b_{bp}$  changes is particularly important to reduce Chl errors or inconsistencies either in one ocean basin or across multiple basins. *Dierssen* [2010] showed that for low Chl values ( $< 0.2\text{--}0.4 \text{ mg m}^{-3}$ ),  $b_{bp}(532)$  may increase by several fold from the North Atlantic to the California coastal waters for the same Chl, and  $b_{bp}(532)$  in the same ocean basin may also remain relatively stable when Chl varied substantially. Similarly, *Loisel et al.* [2002] showed seasonal shifts of  $b_{bp}(490)/\text{Chl}$  from SeaWiFS monthly data for both the North Atlantic and North Pacific, with their relative ratios varying between  $\sim 0.6$  and  $\sim 1.7 (\times 10^{-2} (\text{m}^{-1}/\text{mg m}^{-3}))$ , a change of about threefold. Figure 8b suggests that for a threefold

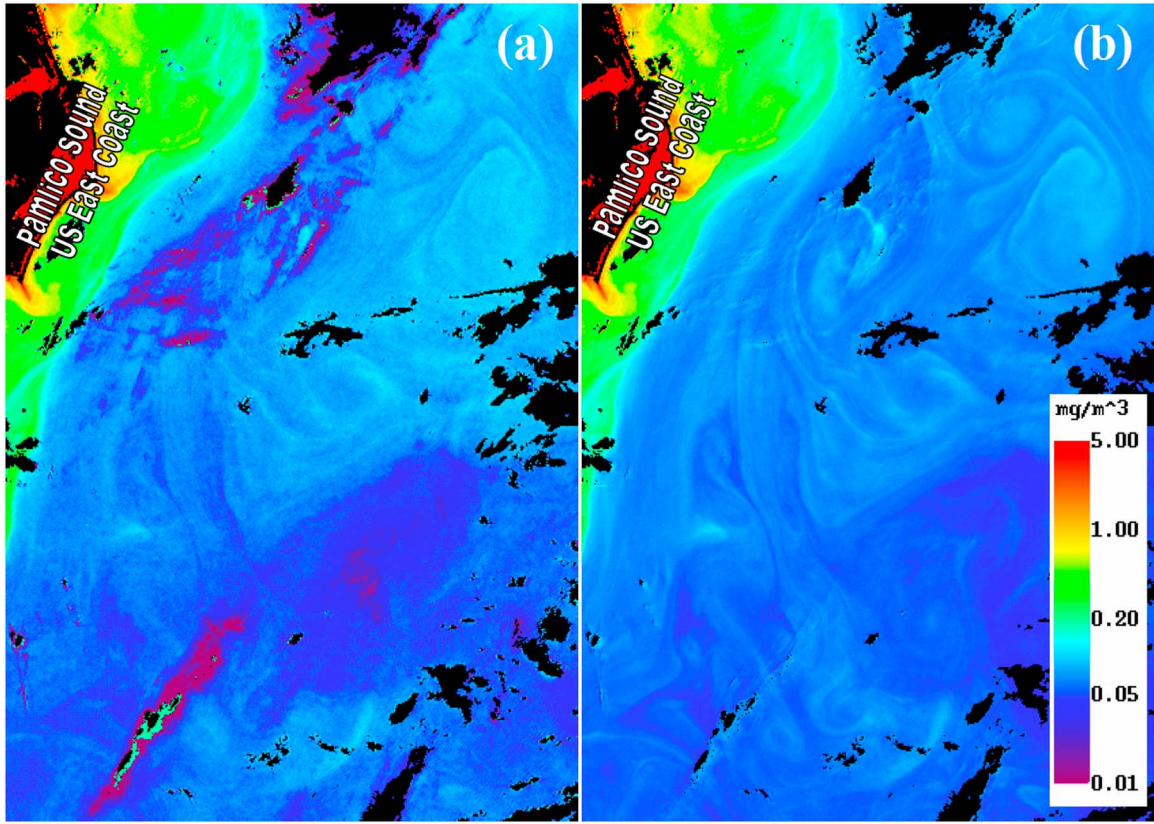


**Figure 15.** Comparison between SeaWiFS Level-2 (a)  $\text{Chl}_{\text{OC}4}$  and (b)  $\text{Chl}_{\text{OCI}}$  over the western North Atlantic Ocean. SeaWiFS data were collected on 1 June 2004 (17:15 UT) and processed with SeaDAS6.1. The Level-2 quality control flags were turned off to show the circulation features. Note that some eddy features are clearly revealed in the  $\text{Chl}_{\text{OCI}}$  image but absent in the  $\text{Chl}_{\text{OC}4}$  image because of noise and residual errors in atmospheric correction and other corrections.

change between 0.175 and 0.525 on the  $x$  axis, relative errors in  $\text{Chl}_{\text{CI}}$  are mostly within  $\pm 10\%$  for  $\text{Chl} \leq 0.3 \text{ mg m}^{-3}$ , while the relative errors in  $\text{Chl}_{\text{OC}4}$  nearly doubled. Thus, the CIA can reduce backscattering-induced errors in the Chl retrieval for oligotrophic waters.

[58] Although the accuracy of the CIA appears to be higher than the SeaWiFS OC4 algorithm (Figure 4) and MODIS/Aqua OC3 algorithm (Figure 5), it is indeed difficult to evaluate the absolute algorithm accuracy for low concentrations. This is primarily due to the lack of sufficient high-quality in situ data. The entire SeaBASS archive is restricted to  $\text{Chl} \geq 0.02 \text{ mg m}^{-3}$ , and only a limited number of stations had Chl between 0.02 and  $0.05 \text{ mg m}^{-3}$ . Laboratory measurement errors in determining Chl from seawater samples, using either fluorometric or HPLC methods, could be up to 50% from earlier reports [Trees *et al.*, 1985; Kumari, 2005]. A more recent comparison between fluorometric and HPLC measurements suggested that these errors could be much smaller [Werdell and Bailey, 2005], yet field measurements in the Southern Ocean still showed some degree of uncertainties for low concentrations [Marrari *et al.*, 2006]. The errors in these ground truth data further weaken the statistical robustness of the validation results when only several points are available. Future efforts may emphasize on the oligotrophic ocean gyres to collect more in situ data

in this range. Because most commercial in situ fluorometers have a precision and also a detection limit of about  $0.01 \text{ mg m}^{-3}$ , accurate in situ measurement for this range is extremely difficult. While new sensors may be developed to increase the precision and accuracy, our current emphasis is on data consistency across various spatial and temporal scales, for which the CIA appears to yield better performance than the band-ratio algorithms.

[59] Despite such improved performance in the CIA, all potential artifacts or uncertainties for empirical algorithms, as discussed and demonstrated in the refereed literature [IOC/CG, 2000, 2006; Dierssen, 2010], still exist (although maybe to a lesser degree than band-ratio algorithms, as shown in the algorithm sensitivity to  $b_{\text{bp}}$  variability). Both CI and band ratio provide a measure of the spectral change of  $R_{\text{rs}}$  (either difference or ratio). While most of such changes could be related to phytoplankton (i.e., Chl), they could also be modulated by changes in CDOM or other OACs. In addition, all these empirical algorithms assume, implicitly, a stable covariation of the chlorophyll-specific absorption coefficient with Chl. The ultimate way to improve Chl retrievals in the global oceans may still be to account for all these variability explicitly through semianalytical inversions, but this is out of the scope of the present work. The semianalytical algorithms, at least in their present forms,

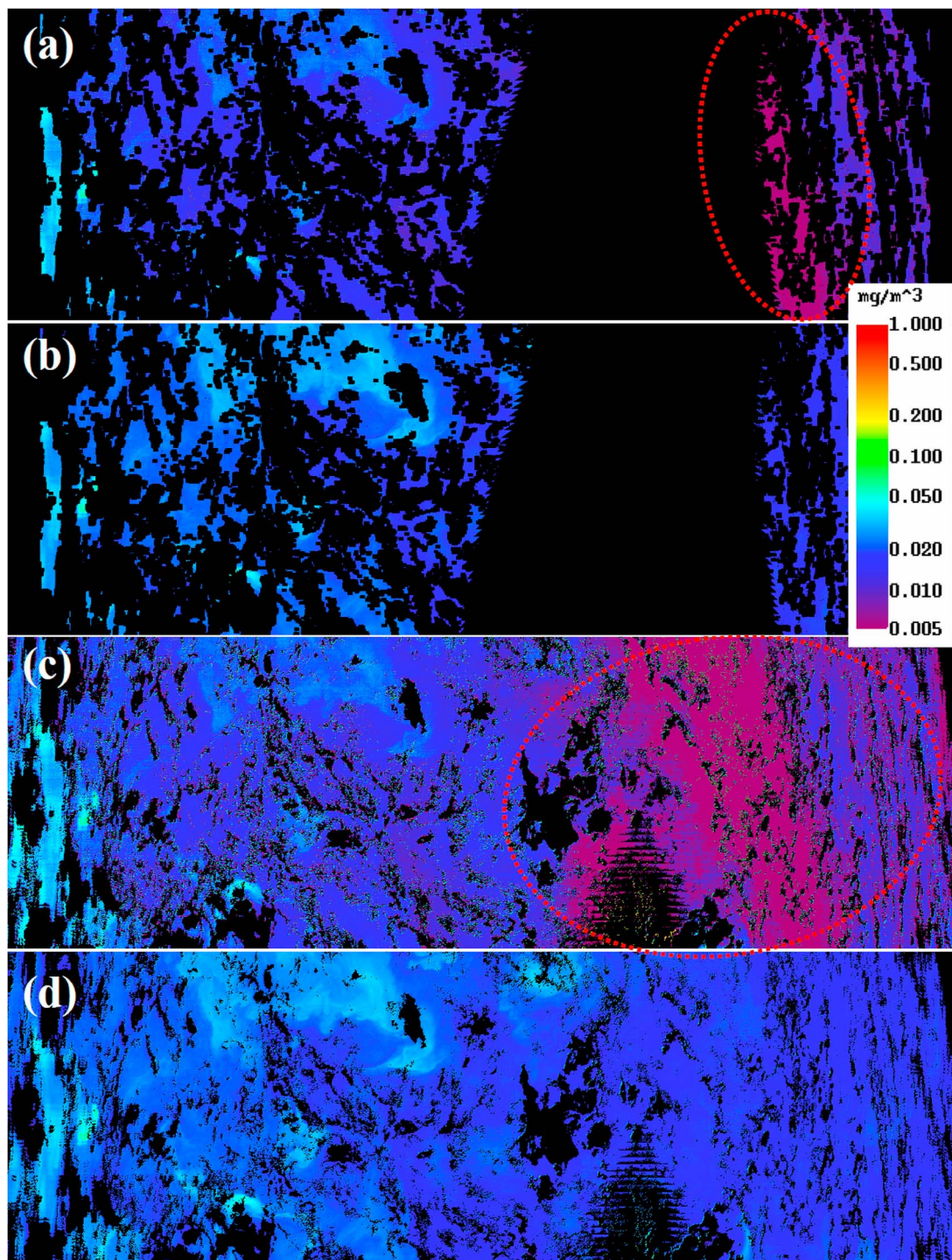


**Figure 16.** MODIS/Aqua Level 2 ChlOC<sub>3</sub> and ChlOC<sub>1</sub> derived from a subregion in the South Pacific Gyre (about 2200 × 440 km centered at 25.2°S, 110.8°W) on 4 March 2003 (21:10 UT). (a and c) The default ChlOC<sub>3</sub> when the quality control flags are on and off, respectively. (b and d) The corresponding ChlOC<sub>1</sub> images.

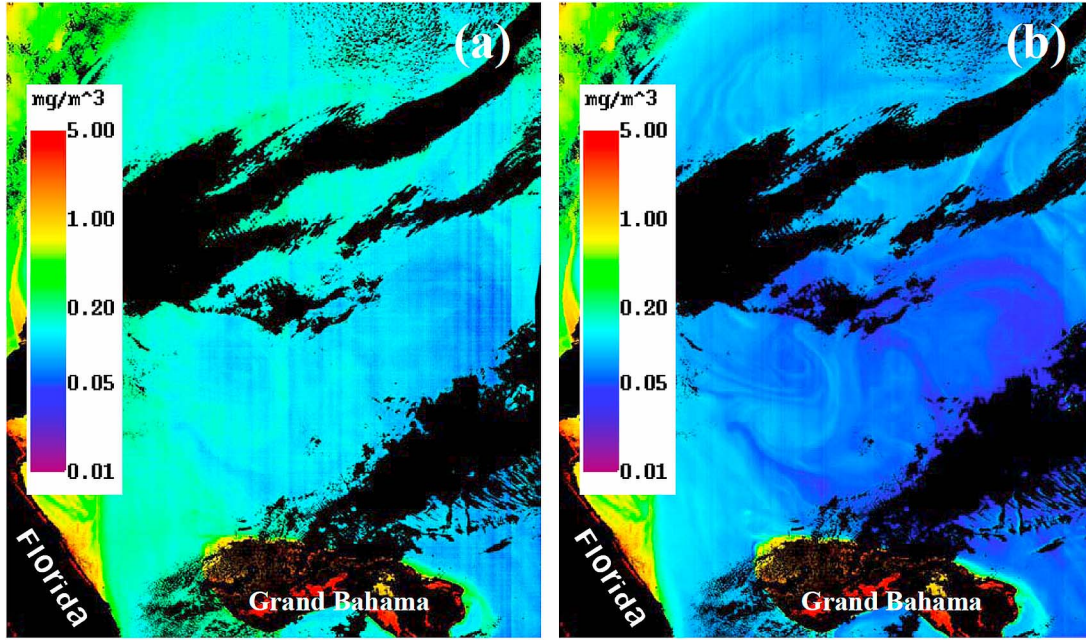


**Figure 17.** Comparison between MERIS full-resolution (a)  $\text{Chl}_{\text{OC}3}$  and (b)  $\text{Chl}_{\text{OCI}}$  over the western North Atlantic Ocean. MERIS data were collected on 7 May 2011 (15:21 UT) and processed with SeaDAS6.1. Note that most speckling and vertical striping noise in the  $\text{Chl}_{\text{OC}3}$  image has been removed in the  $\text{Chl}_{\text{OCI}}$  image, where several eddy and circulation features can be better observed. For demonstration purpose, MERIS full-resolution (FR) data at 300-m nominal resolution were used here. At reduced resolution (RR at 1.2 km), signal-to-noise ratio was significantly higher, leading to much less noise, yet the principle of noise reduction using the OCI algorithm was the same. Furthermore, although the same algorithm coefficients for SeaWiFS were used,  $\text{Chl}_{\text{OCI}}$  values in offshore water appear to be closer than  $\text{Chl}_{\text{OC}3}$  to those from SeaWiFS for the same region during similar periods (Figure 13).

however, are not immune to the problems shown in Figure 1d, where  $R_{rs}$  data (input of the algorithms) contain substantial noise and errors. These errors must be corrected in order to improve the performance of semianalytical algorithms. Likewise, algorithms for many other ocean color products (e.g., IOPs, particulate organic carbon, particulate inorganic carbon) rely heavily on accurate  $R_{rs}(\lambda)$ , whose performance may also be improved once the errors in the satellite-derived  $R_{rs}(\lambda)$  are reduced.

[60] All above analyses were restricted to SeaWiFS GAC data and MODIS LAC data. However, application of the same CIA algorithm to SeaWiFS LAC data showed similar improvements over image quality. Figure 15 shows an example of the comparison of  $\text{Chl}_{\text{OC}4}$  and  $\text{Chl}_{\text{OCI}}$  using SeaWiFS Level-2 LAC data. Clearly, all instrument/algorithm artifacts shown in the GAC data (Figure 1) also exist in the LAC data (to a lesser degree), but these artifacts can be effectively removed by the CIA.

[61] Analyses of MODIS/Aqua Level-2 data for a  $20^\circ \times 20^\circ$  box in the South Pacific Gyre (745 images in 2002) showed similar results as for SeaWiFS. Figure 12b shows that, although the speckling errors are reduced for MODIS  $\text{Chl}_{\text{OC}3}$  relative to SeaWiFS  $\text{Chl}_{\text{OC}4}$  (MODIS/Aqua instrument signal-to-noise ratio is about 2–3 times higher than that of SeaWiFS), the general pattern remains the same, i.e., increased speckling errors with decreasing concentrations. MODIS  $\text{Chl}_{\text{OCI}}$ , in contrast, shows relatively stable and much lower speckling errors. Nearly all data points with  $\text{Chl}_{\text{OC}3} < 0.01 \text{ mg m}^{-3}$  have been raised in  $\text{Chl}_{\text{OCI}}$ , and this

is likely to be real, as the “clearest natural waters” had Chl values of  $\sim 0.02 \text{ mg mg}^{-3}$  [Morel et al., 2007b].

[62] Figure 16 shows that MODIS/Aqua  $\text{Chl}_{\text{OC}3}$  data are not immune to noise and algorithm errors even after all suspicious data (associated with the various quality control flags) are discarded. In contrast, the CIA successfully corrected these suspicious data to reasonable levels, as gauged from nearby pixels and adjacent images. This result explains the histogram shift between  $\text{Chl}_{\text{OC}3}$  and  $\text{Chl}_{\text{CI}}$  for extremely low values in Figure 12b. Furthermore, even when all the quality control flags are turned off (i.e., all low-quality nonzero data are included), the CIA appears to perform well on all those flagged pixels (Figures 16c and 16d), indicating that the  $R_{rs}(\lambda)$  errors from those pixels are spectrally related so that the CIA could remove these errors, at least to the first order. This suggests that the CIA may also result in more spatial coverage, once appropriate flags are determined to relax the quality control criteria.

## 9.2. Applications to Other Ocean Color Instruments

[63] The improved performance of the CIA over OCx for low concentrations appears to be universal across sensors, although the regression coefficients may need to be adjusted to account for sensor specifics.

[64] Figure 17 shows an example of how the CIA (same coefficients used for SeaWiFS) improves MERIS image quality when compared with the default band-ratio algorithm. The reduction of speckling noise and striping noise is apparent in the  $\text{Chl}_{\text{OCI}}$  image, with more coherent eddy

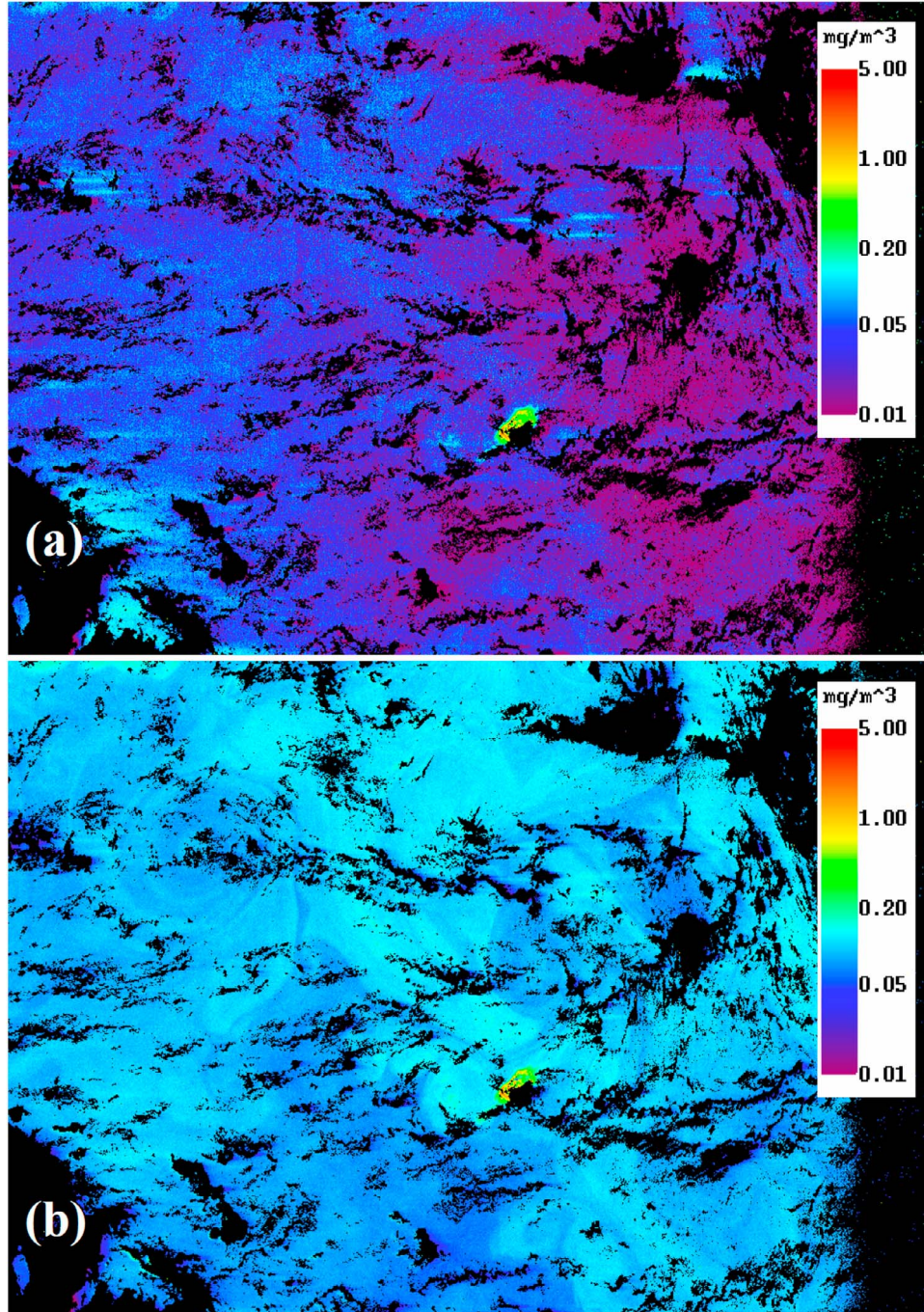


**Figure 18.** Comparison between CZCS Level-2 (a)  $\text{Chl}_{\text{OC}2}$  and (b)  $\text{Chl}_{\text{OC}1}$  over the western North Atlantic Ocean (about  $30^{\circ}$ – $36^{\circ}\text{N}$ ,  $70^{\circ}$ – $60^{\circ}\text{W}$ ). CZCS data were collected on 31 July 1983 (16:02 UT) and processed with SeaDAS6.1. Note that all eddy and circulation features in the  $\text{Chl}_{\text{OC}1}$  image are completely absent in the  $\text{Chl}_{\text{OC}2}$  image.

features observed. More profound improvement has also been found for CZCS (Figure 18). CZCS is an 8-bit instrument with a much lower signal-to-noise ratio (about 3 times lower than SeaWiFS), and the band-ratio algorithm resulted in significant speckling noise and other errors (Figure 18a), where no ocean feature can be observed. In contrast, most of these errors have been removed by the CIA, leading to clear eddy and circulation features in the North Atlantic

oligotrophic ocean. Furthermore, the general gradient from west to east in Figure 18a, a result of algorithm artifact, has been successfully removed in Figure 18b.

[65] The tolerance of the CIA to various noise and errors is particularly useful for instruments with sensitivity much lower than that of MODIS and SeaWiFS, as demonstrated in Figure 18. The Visible/Infrared Imager/Radiometer Suite of the National Polar-orbiting Operational Environmental

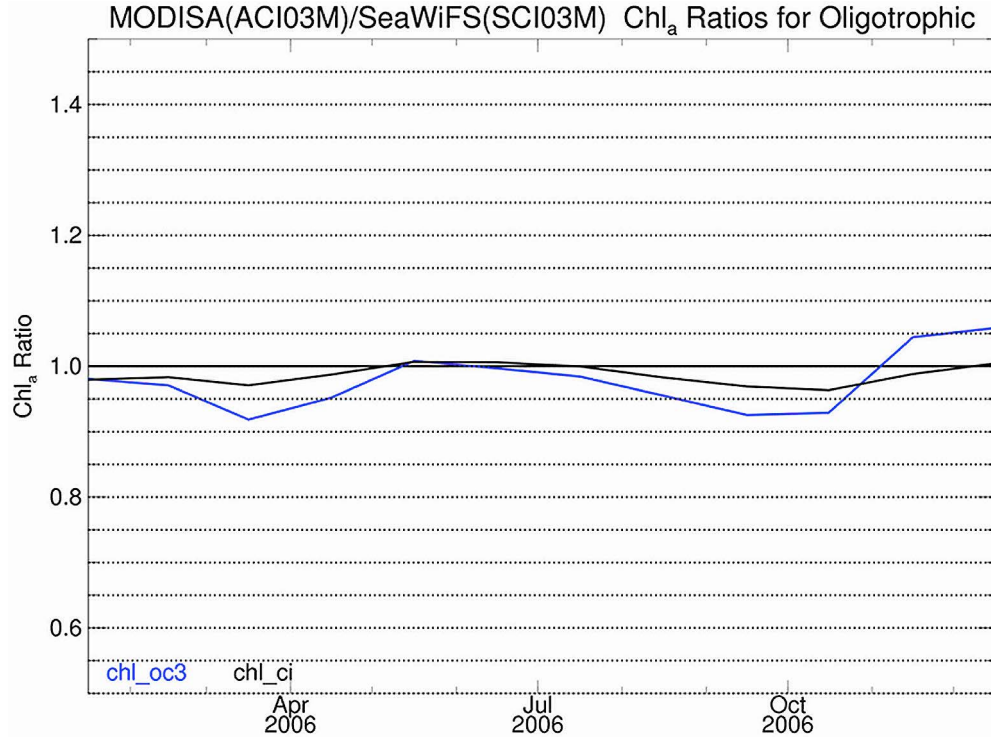


**Figure 19.** Mean Chl ratio over global oligotrophic oceans between MODIS/Aqua and SeaWiFS estimates using the OCx (blue) and CI (black) algorithms. Here “oligotrophic” is defined as all 9 km pixels with SeaWiFS mission mean Chl  $\leq 0.1 \text{ mg m}^{-3}$ .

Satellite System Preparatory Project (NPP), launched in space on 25 October 2011, was specified to have sensitivity lower than SeaWiFS. Thus, significant noise will result from band-ratio Chl algorithms for low concentrations, yet the CIA is likely to remove all these artifacts.

### 9.3. Chl Climate Data Record

[66] Although the absolute accuracy in the retrieved Chl<sub>OCI</sub> for ocean color instruments other than SeaWiFS and MODIS/Aqua has not been evaluated, we believe that once algorithm coefficients are tuned for the particular instruments or the satellite-derived  $R_{rs}(\lambda)$  are tuned to the SeaWiFS wavelengths, a significant improvement in product accuracy, in addition to improved image quality, can be achieved. Such an improvement may lead to more consistent observations between different instruments. For example, after a slight adjustment to convert the MODIS/Aqua  $R_{rs}(547)$  to  $R_{rs}(555)$  and application of the same CIA and coefficients (equation (4)) to the global data for 2006, the mean ratio between MODIS and SeaWiFS Chl over the global oligotrophic oceans shows much less seasonal variability and is closer to 1.0 from the CIA than from the OCx algorithms (Figure 19). Such an improvement is even more profound when data distributions, rather than a global mean ratio, are examined. Figure 20 shows the data distributions for all deep waters ( $>200 \text{ m}$ ) from the band ratio (OCx) and CI algorithms using all SeaWiFS and MODIS/Aqua data collected during November 2006. Although there is a slight offset of  $0.01\text{--}0.02 \text{ mg m}^{-3}$  in the global mean and median values between the two algorithm results (Figures 20a and

20b, respectively), the CIA (after blending with the OCx for Chl  $> 0.25 \text{ mg m}^{-3}$ ) resulted in nearly identical histograms between SeaWiFS and MODIS/Aqua measurements, a significant improvement in cross-sensor data consistency compared with the OCx results. Figure 21 further shows the spatial patterns of the improved data consistency between the two instruments for 2 months in 2006. The SeaWiFS/MODISA Chl ratios from the OCx algorithms often showed a substantial departure from 1.0 with coherent spatial patterns, and such patterns varied with time. In contrast, the same ratios from the OCI algorithm were much closer to 1.0, with most of the spatial and temporal patterns removed. Analyses for other months of 2006 showed similar improvements. Although we are still performing an extensive evaluation of the new algorithm for the global ocean using all SeaWiFS and MODIS/Aqua data, the improved consistency between SeaWiFS and MODIS/Aqua measurements from these preliminary results is indeed encouraging and may eventually lead to a better multisensor Chl climate data record for studies of the ocean’s long-term biogeochemical changes in response to climate variability [Antoine et al., 2005; Gregg et al., 2005; Gregg and Casey, 2010; Maritorena et al., 2010]. The reduction in spatially coherent inconsistency patterns, as demonstrated in Figure 21, may also have profound impacts on basin-scale and cross-basin studies of ocean changes and processes.

### 9.4. Other Applications

[67] Studies of the ocean’s biogeochemistry call for the highest accuracy in data products. For many other

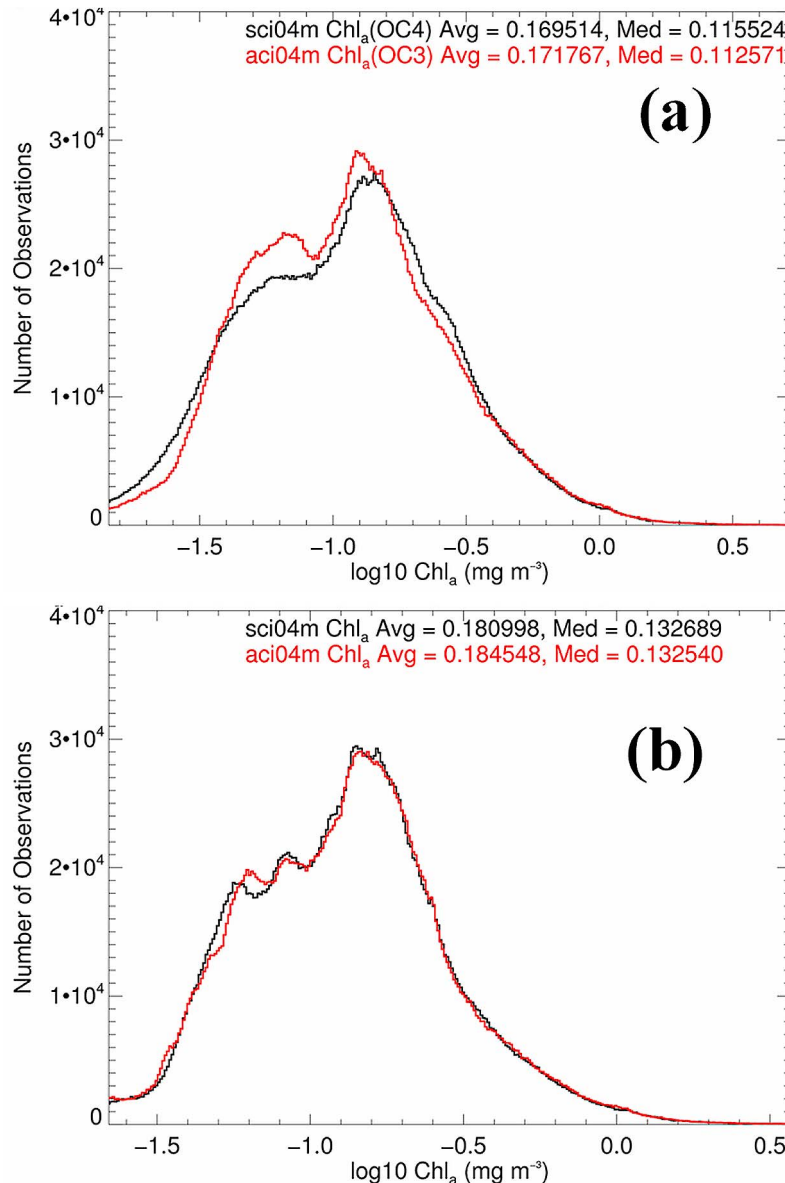


**Figure 20.** Chl distributions in the global deep oceans ( $>1000$  m) during November 2006, as derived from SeaWiFS (black) and MODIS/Aqua (red) measurements. Results are from (a) the OCx band-ratio algorithms and (b) the CI algorithm (blended with the OCx algorithms for  $\text{Chl} > 0.25 \text{ mg m}^{-3}$ ). Note the offset of  $0.01\text{--}0.02 \text{ mg m}^{-3}$  in the global mean and median values between Figures 20a and 20b. Results from other months of 2006 show similar improvements in histogram consistency.

applications, such a strict requirement may often be relaxed. For example, tracking of oil pollution requires timely knowledge on major ocean circulation features, including eddies [Hu, 2011; Liu *et al.*, 2011]. The various examples shown in Figures 15–18 prove that the CIA can lead to significantly improved image quality for feature recognition when individual images are used. This is due to its ability to reduce noise and errors as well as to recover most of the flagged (i.e., suspicious) pixels. Some of the eddy features are completely absent in the  $\text{Chl}_{\text{OCX}}$  images because of noise and algorithm errors, regardless of the color stretch, but are vividly revealed in the  $\text{Chl}_{\text{OCI}}$  images. This ability will

greatly facilitate studies of eddy dynamics [e.g., Lehahn *et al.*, 2007; Rossby *et al.*, 2011] in the oligotrophic oceans.

## 10. Conclusion

[68] A novel three-band reflectance difference algorithm, namely, a CIA, to estimate surface chlorophyll *a* concentrations from satellite ocean color measurements has been shown superior to the existing band-ratio algorithms in reducing uncertainties for  $\text{Chl} \leq 0.25 \text{ mg m}^{-3}$ , corresponding to about 78% of the global ocean. This was somehow a surprise, given the known artifacts of two-band difference

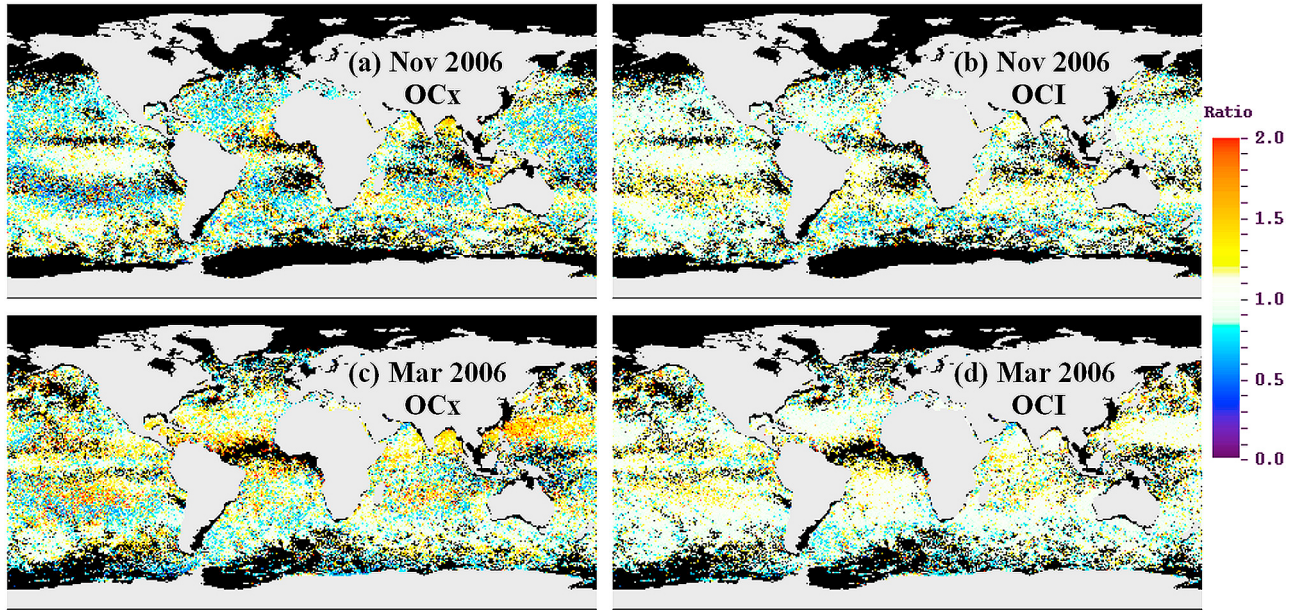


**Figure 21.** SeaWiFS/MODISA Chl ratios for global oceans ( $>200$  m) derived from the band-ratio OCx algorithms (OC4 for SeaWiFS and OC3 for MODISA/Aqua) and from the OCI algorithm for (a and b) November 2006 and (c and d) March 2006. Black means no data.

algorithms proposed three decades ago. We attribute the success of the CIA to the new design of adding a third band in the red to the blue-green bands. This addition enables the CIA to relax the requirements of spectrally flat errors for the two-band difference algorithms to spectrally linear errors for the CIA and also increases the stability of algorithm performance over backscattering variability of the ocean. The improved performance of the CIA over the existing band-ratio algorithms has been demonstrated in all measures, from global validations using in situ data, atmospheric correction, and bio-optical simulations to satellite image analysis. The CIA also appears to improve data consistency between different instruments for oligotrophic oceans, and such consistency may lead to an improved Chl climate data record from multiple sensors for future ocean-color continuity missions. We expect to implement the CIA for multisensor global processing for oligotrophic oceans to further test its robustness, which might lead to different and potentially improved spatial and temporal patterns of Chl in response to long-term climate changes and short-term climate variability.

[69] **Acknowledgments.** This work is impossible without the collective effort from the entire ocean color community, from sensor calibration, field campaign, algorithm development, product validation, to data sharing. We are particularly thankful to the researchers who collected and contributed in situ bio-optical data to the SeaBASS archive, as well as to the NASA/GSFC OBPG team (Sean Bailey and Jeremy Werdell) who quality controlled, maintained, and distributed the data set for community use. We thank Howard Gordon (University of Miami) for the useful discussions on atmospheric correction uncertainties. We also thank the NASA/GSFC for sharing the global ocean color data at all data levels. Financial support has been provided by the NASA Ocean Biology and Biogeochemistry (OBB) program (Hu, Lee, Franz), Gulf of Mexico program (Hu, Lee), the Energy and Water Cycle program (Lee, Hu), and the Naval Research Lab (Lee). We are indebted to two anonymous reviewers who provided numerous suggestions to improve the quality of this work.

## References

- Ahmad, Z., B. A. Franz, C. R. Charles, E. J. Kwiatkowska, J. Werdell, E. P. Shettle, and B. N. Holben (2010), New aerosol models for the retrieval of aerosol optical thickness and normalized water-leaving radiances from the SeaWiFS and MODIS sensors over coastal regions and open oceans, *Appl. Opt.*, **49**, 5545–5560, doi:10.1364/AO.49.005545.
- Antoine, D., A. Morel, H. R. Gordon, V. F. Banzon, and R. H. Evans (2005), Bridging ocean color observations of the 1980s and 2000s in search of long-term trends, *J. Geophys. Res.*, **110**, C06009, doi:10.1029/2004JC002620.
- Arvesen, J. C., J. P. Millard, and E. C. Weaver (1973), Remote sensing of chlorophyll and temperature in marine and fresh waters, *Acta Astronaut.*, **18**, 229–239.
- Bailey, S. W., B. A. Franz, and P. J. Werdell (2010), Estimation of near-infrared water-leaving reflectance for satellite ocean color data processing, *Opt. Express*, **18**, 7521–7527, doi:10.1364/OE.18.007521.
- Barnard, A. H., J. R. Zaneveld, and W. S. Pegau (1999), In situ determination of the remotely sensed reflectance and the absorption coefficient: Closure and inversion, *Appl. Opt.*, **38**, 5108–5117, doi:10.1364/AO.38.005108.
- Behrenfeld, M., R. O’Malley, D. A. Siegel, C. R. McClain, J. Sarmiento, G. Feldman, P. Falkowski, E. Boss, and A. Milligan (2006), Climate-driven trends in contemporary ocean productivity, *Nature*, **444**, 752–755, doi:10.1038/nature05317.
- Bricaud, A., M. Babin, A. Morel, and H. Claustre (1995), Variability in the chlorophyll-specific absorption coefficients of natural phytoplankton: Analysis and parameterization, *J. Geophys. Res.*, **100**(C7), 13,321–13,332, doi:10.1029/95JC00463.
- Brown, C., Y. Huot, P. J. Werdell, B. Gentili, and H. Claustre (2008), The origin and global distribution of second order variability in satellite ocean color, *Remote Sens. Environ.*, **112**, 4186–4203, doi:10.1016/j.rse.2008.06.008.
- Campbell, J. W. (1995), The lognormal distribution as a model for bio-optical variability in the sea, *J. Geophys. Res.*, **100**(C7), 13,237–13,254, doi:10.1029/95JC00458.
- Campbell, J. W., and W. E. Esaias (1983), Basis for spectral curvature algorithms in remote sensing of chlorophyll, *Appl. Opt.*, **22**, 1084–1093, doi:10.1364/AO.22.001084.
- Carder, K. L., F. R. Chen, Z. P. Lee, S. K. Hawes, and D. Kamikowski (1999), Semianalytic moderate-resolution imaging spectrometer algorithms for chlorophyll  $a$  and absorption with bio-optical domains based on nitrate-depletion temperatures, *J. Geophys. Res.*, **104**, 5403–5421, doi:10.1029/1998JC900082.

- Clark, D. K., E. T. Baker, and A. E. Strong (1980), Upwelled spectral radiance distribution in relation to particulate matter in sea water, *Boundary Layer Meteorol.*, **18**, 287–298, doi:10.1007/BF00122025.
- Clarke, G. K., G. C. Ewing, and C. J. Lorenzen (1970), Spectra of backscattered light from the sea obtained from aircraft as a measure of chlorophyll concentration, *Science*, **167**, 1119–1121, doi:10.1126/science.167.3921.1119.
- Claustre, H., and S. Maritorena (2003), The many shades of ocean blue, *Science*, **302**, 1514–1515, doi:10.1126/science.1092704.
- Dierssen, H. M. (2010), Perspectives on empirical approaches for ocean color remote sensing of chlorophyll in a changing climate, *Proc. Natl. Acad. Sci. U. S. A.*, **107**, 17,073–17,078, doi:10.1073/pnas.0913800107.
- Dierssen, H. M., R. C. Smith, and M. Verner (2002), Glacial meltwater dynamics in coastal waters west of the Antarctic peninsula, *Proc. Natl. Acad. Sci. U. S. A.*, **99**, 1790–1795, doi:10.1073/pnas.032206999.
- Franz, B. A., S. W. Bailey, P. J. Werdell, and C. R. McClain (2007), Sensor-independent approach to the vicarious calibration of satellite ocean color radiometry, *Appl. Opt.*, **46**, 5068–5082, doi:10.1364/AO.46.005068.
- Frouin, R. (1997), NDPI for satellite ocean color applications, paper presented at Fourth International POLDER Science Working Team Meeting, Boussens, France, 25–28 Nov.
- Frouin, R., M. Schwindling, and P.-Y. Deschamps (1996), Spectral reflectance of sea foam in the visible and near-infrared: In situ measurements and remote sensing implications, *J. Geophys. Res.*, **101**, 14,361–14,371, doi:10.1029/96JC00629.
- Gordon, H. R. (1997), Atmospheric correction of ocean color imagery in the Earth Observing System era, *J. Geophys. Res.*, **102**, 17,081–17,106, doi:10.1029/96JD02443.
- Gordon, H. R., and D. K. Clark (1980), Remote sensing optical properties of a stratified ocean: An improved interpretation, *Appl. Opt.*, **19**, 3428–3430, doi:10.1364/AO.19.003428.
- Gordon, H. R., and D. K. Clark (1981), Clear water radiances for atmospheric correction of coastal zone color scanner imagery, *Appl. Opt.*, **20**, 4175–4180, doi:10.1364/AO.20.004175.
- Gordon, H. R., and A. Y. Morel (1983), *Remote Assessment of Ocean Color for Interpretation of Satellite Visible Imagery. A Review*, 114 pp., Springer, New York.
- Gordon, H. R., and M. Wang (1994a), Retrieval of water-leaving radiance and aerosol optical thickness over the oceans with SeaWiFS: A preliminary algorithm, *Appl. Opt.*, **33**, 443–452, doi:10.1364/AO.33.000443.
- Gordon, H. R., and M. Wang (1994b), Influence of oceanic whitecaps on atmospheric correction of SeaWiFS, *Appl. Opt.*, **33**, 7754–7763, doi:10.1364/AO.33.007754.
- Gower, J., S. King, G. Borstad, and L. Brown (2005), Detection of intense plankton blooms using the 709 nm band of the MERIS imaging spectrometer, *Int. J. Remote Sens.*, **26**, 2005–2012, doi:10.1080/01431160500075857.
- Gregg, W. W., and N. W. Casey (2004), Global and regional evaluation of the SeaWiFS chlorophyll dataset, *Remote Sens. Environ.*, **93**, 463–479, doi:10.1016/j.rse.2003.12.012.
- Gregg, W. W., and N. W. Casey (2010), Improving the consistency of ocean color data: A step toward climate data records, *Geophys. Res. Lett.*, **37**, L04605, doi:10.1029/2009GL041893.
- Gregg, W. W., N. W. Casey, and C. R. McClain (2005), Recent trends in global ocean chlorophyll, *Geophys. Res. Lett.*, **32**, L03606, doi:10.1029/2004GL021808.
- Hooker, S. B., G. Lazin, G. Zibordi, and S. McLean (2002), An evaluation of above- and in-water methods for determining water-leaving radiances, *J. Atmos. Oceanic Technol.*, **19**, 486–515, doi:10.1175/1520-0426(2002)019<0486:AOEAAI>2.0.CO;2.
- Hovis, W. A., and K. C. Leung (1977), Remote sensing of ocean color, *Opt. Eng.*, **16**, 153–166.
- Hu, C. (2009), A novel ocean color index to detect floating algae in the global oceans, *Remote Sens. Environ.*, **113**, 2118–2129.
- Hu, C. (2011), An empirical approach to derive MODIS ocean color patterns under severe sun glint, *Geophys. Res. Lett.*, **38**, L01603, doi:10.1029/2010GL045422.
- Hu, C., K. L. Carder, and F. E. Muller-Karger (2001), How precise are SeaWiFS ocean color estimates? Implications of digitization-noise errors, *Remote Sens. Environ.*, **76**, 239–249, doi:10.1016/S0034-4257(00)00206-6.
- Hu, C., F. E. Muller-Karger, D. C. Biggs, K. L. Carder, B. Nababan, D. Nadeau, and J. Vanderbloemen (2003), Comparison of ship and satellite bio-optical measurements on the continental margin of the NE Gulf of Mexico, *Int. J. Remote Sens.*, **24**, 2597–2612, doi:10.1080/0143116031000067007.
- Hu, C., Z. Lee, F. E. Muller-Karger, K. L. Carder, and J. J. Walsh (2006), Ocean color reveals phase shift between marine plants and yellow substance, *IEEE Geosci. Remote Sens. Lett.*, **3**, 262–266, doi:10.1109/LGRS.2005.862527.
- International Ocean-Colour Coordinating Group (IOCCG) (2000), *Remote Sensing of Ocean Color in Coastal, and Other Optically Complex, Waters*, IOCCG Rep. 3, edited by S. Sathyendranath, Dartmouth, N. S., Canada.
- International Ocean-Colour Coordinating Group (IOCCG) (2006), *Remote Sensing of Inherent Optical Properties: Fundamentals, Tests of Algorithms, and Applications*, IOCCG Rep. 5, edited by Z.-P. Lee, Dartmouth, N. S., Canada.
- Kahru, M., and B. G. Mitchell (1999), Empirical chlorophyll algorithm and preliminary SeaWiFS validation for the California Current, *Int. J. Remote Sens.*, **20**(17), 3423–3429, doi:10.1080/014311699211453.
- Kumari, B. (2005), Comparison of high performance liquid chromatography and fluorometric ocean colour pigments, *J. Indian Soc. Remote Sens.*, **33**, 541–546, doi:10.1007/BF02990739.
- Lee, Z., and K. L. Carder (2000), Band-ratio or spectral-curvature algorithms for satellite remote sensing?, *Appl. Opt.*, **39**, 4377–4380, doi:10.1364/AO.39.004377.
- Lee, Z., R. Arnone, C. Hu, P. J. Werdell, and B. Lubac (2010), Uncertainties of optical parameters and their propagations in an analytical ocean color inversion algorithm, *Appl. Opt.*, **49**, 369–381, doi:10.1364/AO.49.000369.
- Lee, Z.-P., K. Du, K. Voss, G. Zibordi, B. Lubac, R. Arnone, and A. Weidemann (2011), An inherent-optical-property-centered approach to correct the angular effects in water-leaving radiance, *Appl. Opt.*, **50**, 3155–3167, doi:10.1364/AO.50.003155.
- Lehahn, Y., F. d'Ovidio, M. Levy, and E. Heifetz (2007), Stirring of the northeast Atlantic spring bloom: A Lagrangian analysis based on multisatellite data, *J. Geophys. Res.*, **112**, C08005, doi:10.1029/2006JC003927.
- Letelier, R. M., and M. R. Abbott (1996), An analysis of chlorophyll fluorescence algorithms for the Moderate Resolution Imaging Spectrometer (MODIS), *Remote Sens. Environ.*, **58**, 215–223, doi:10.1016/S0034-4257(96)00073-9.
- Liu, Y., R. H. Weisberg, C. Hu, and L. Zheng (2011), Tracking the Deep-water Horizon oil spill: A modelling perspective, *Eos Trans. AGU*, **92**(6), 45.
- Loisel, H., J.-M. Nicolas, P.-Y. Deschamps, and R. Frouin (2002), Seasonal and inter-annual variability of particulate organic matter in the global ocean, *Geophys. Res. Lett.*, **29**(24), 2196, doi:10.1029/2002GL015948.
- Maritorena, S., D. A. Siegel, and A. Peterson (2002), Optimization of a semi-analytical ocean color model for global scale applications, *Appl. Opt.*, **41**, 2705–2714, doi:10.1364/AO.41.002705.
- Maritorena, S., O. Hembise Fanton d'Andon, A. Mangin, and D. A. Siegel (2010), Merged satellite ocean color data products using a bio-optical model: Characteristics, benefits and issues, *Remote Sens. Environ.*, **114**(8), 1791–1804, doi:10.1016/j.rse.2010.04.002.
- Marrari, M., C. Hu, and K. Daly (2006), Validation of SeaWiFS chlorophyll-a concentrations in the Southern Ocean: A revisit, *Remote Sens. Environ.*, **105**, 367–375, doi:10.1016/j.rse.2006.07.008.
- McClain, C. R. (2009), A decade of satellite ocean color observations, *Annu. Rev. Mar. Sci.*, **1**, 19–42, doi:10.1146/annurev.marine.010908.163650.
- McClain, C. R., G. C. Feldman, and S. B. Hooker (2004a), An overview of the SeaWiFS project and strategies for producing a climate research quality global ocean bio-optical time series, *Deep Sea Res., Part II*, **51**, 5–42, doi:10.1016/j.dsr2.2003.11.001.
- McClain, C. R., S. R. Signorini, and J. R. Christian (2004b), Subtropical gyre variability observed by ocean-color satellites, *Deep Sea Res., Part II*, **51**, 281–301, doi:10.1016/j.dsr2.2003.08.002.
- McKee, D., A. Cunningham, and A. Dudek (2007), Optical water type discrimination and tuning remote sensing band-ratio algorithms: Application to retrieval of chlorophyll and  $K_d(490)$  in the Irish and Celtic Seas, *Estuarine Coastal Shelf Sci.*, **73**, 827–834, doi:10.1016/j.ecss.2007.03.028.
- Mitchell, B. G., and M. Kahru (2009), Bio-optical algorithms for ADEOS-2 GLI, *J. Remote Sens. Soc. Jpn.*, **29**, 80–85.
- Morel, A. (1974), Optical properties of pure water and pure sea water, in *Optical Aspects of Oceanography*, edited by N. G. Jerlov and E. S. Nielsen, pp. 1–24, Academic, New York.
- Morel, A. Y. (1980), In-water and remote measurement of ocean color, *Boundary Layer Meteorol.*, **18**, 177–201, doi:10.1007/BF00121323.
- Morel, A. (2009), Are the empirical relationships describing the bio-optical properties of case 1 waters consistent and internally compatible?, *J. Geophys. Res.*, **114**, C01016, doi:10.1029/2008JC004803.
- Morel, A., and B. Gentili (1993), Diffuse reflectance of oceanic waters (2), Bi-directional aspects, *Appl. Opt.*, **32**, 6864–6879, doi:10.1364/AO.32.006864.
- Morel, A., and S. Maritorena (2001), Bio-optical properties of oceanic waters: A reappraisal, *J. Geophys. Res.*, **106**, 7163–7180, doi:10.1029/2000JC000319.

- Morel, A. Y., and L. Prieur (1977), Analysis of variations in ocean color, *Limnol. Oceanogr.*, 22, 709–722, doi:10.4319/lo.1977.22.4.0709.
- Morel, A., Y. Huot, B. Gentili, P. J. Werdell, S. B. Hooker, and B. A. Franz (2007a), Examining the consistency of products derived from various ocean color sensors in open ocean (case 1) waters in the perspective of a multi-sensor approach, *Remote Sens. Environ.*, 111, 69–88, doi:10.1016/j.rse.2007.03.012.
- Morel, A., B. Gentili, H. Claustre, M. Babin, A. Bricaud, J. Ras, and F. Tieche (2007b), Optical properties of the “clearest” natural waters, *Limnol. Oceanogr.*, 52(1), 217–229, doi:10.4319/lo.2007.52.1.0217.
- Mukai, S., I. Sano, and Y. Okada (2000), Inverse problems in the atmosphere-ocean system: Estimation of aerosol characteristics and phytoplankton distribution, *Appl. Math. Comput.*, 116, 93–101, doi:10.1016/S0096-3003(99)00197-6.
- Odriozola, A. L., R. Varela, C. Hu, Y. Astor, L. Lorenzoni, and F. E. Muller-Karger (2007), On the absorption of light in the Orinoco River plume, *Cont. Shelf Res.*, 27, 1447–1464, doi:10.1016/j.csr.2007.01.012.
- O'Reilly, J. E., et al. (2000), SeaWiFS postlaunch calibration and validation analyses, Part 3, *NASA Tech. Memo.*, NASA, TM-2000-206892, vol. 11, 49 pp.
- Polovina, J. J., E. A. Howell, and M. Abecassis (2008), Ocean's least productive waters are expanding, *Geophys. Res. Lett.*, 35, L03618, doi:10.1029/2007GL031745.
- Pope, R., and E. Fry (1997), Absorption spectrum (380–700 nm) of pure waters: II. Integrating cavity measurements, *Appl. Opt.*, 36, 8710–8723, doi:10.1364/AO.36.008710.
- Rossby, T., C. Flagg, P. Ortner, and C. Hu (2011), A tale of two eddies: Diagnosing coherent eddies through acoustic remote sensing, *J. Geophys. Res.*, 116, C12017, doi:10.1029/2011JC007307.
- Sathyendranath, S., L. Prieur, and A. More (1989), A three component model of ocean colour and its application to remote sensing of phytoplankton pigments in coastal waters, *Int. J. Remote Sens.*, 10, 1373–1394, doi:10.1080/01431168908903974.
- Sullivan, J. M., and M. S. Twardowski (2009), Angular shape of the oceanic particulate volume scattering function in the backward direction, *Appl. Opt.*, 48(35), 6811–6819, doi:10.1364/AO.48.006811.
- Tassan, S. (1981), A global sensitivity analysis for the retrieval of chlorophyll concentrations from remote sensed radiances—the influence of wind, in *Oceanography From Space*, edited by J. R. F. Gower, pp. 371–375, Plenum, New York, doi:10.1007/978-1-4613-3315-9\_41.
- Tomlinson, M. C., T. T. Wynne, and R. P. Stumpf (2009), An evaluation of remote sensing techniques for enhanced detection of the toxic dinoflagellate, Karenia brevis, *Remote Sens. Environ.*, 113, 598–609, doi:10.1016/j.rse.2008.11.003.
- Trees, C. C., M. C. Kennicutt, and M. J. Brooks (1985), Errors associated with the standard fluorometric determination of chlorophylls and phaeopigments, *Mar. Chem.*, 17, 1–12, doi:10.1016/0304-4203(85)90032-5.
- Viollier, M., P. Y. Deschamps, and P. Lecomte (1978), Airborne remote sensing of chlorophyll content under cloudy sky as applied to the tropical waters in the Gulf of Guinea, *Remote Sens. Environ.*, 7, 235–248, doi:10.1016/0034-4257(78)90035-4.
- Viollier, M., D. Tanre, and P. Y. Deschamps (1980), An algorithm for remote sensing of water color from space, *Boundary Layer Meteorol.*, 18, 247–267, doi:10.1007/BF00122023.
- Wang, M., and S. W. Bailey (2001), Correction of sun glint contamination on the SeaWiFS ocean and atmosphere products, *Appl. Opt.*, 40, 4790–4798, doi:10.1364/AO.40.004790.
- Werdell, P. J., and S. W. Bailey (2005), An improved in-situ bio-optical data set for ocean color algorithm development and satellite data product validation, *Remote Sens. Environ.*, 98, 122–140, doi:10.1016/j.rse.2005.07.001.
- Yoder, J. A., and M. A. Kennelly (2006), What have we learned about ocean variability from satellite ocean color imagers?, *Oceanography*, 19, 152–171, doi:10.5670/oceanog.2006.98.
- Zhang, X., M. Lewis, and B. Johnson (1998), Influence of bubbles on scattering of light in the ocean, *Appl. Opt.*, 37, 6525–6536, doi:10.1364/AO.37.006525.

B. Franz, NASA GSFC, Greenbelt, MD 20771, USA.

C. Hu, College of Marine Science, University of South Florida, St. Petersburg, FL 33701, USA. (hu@marine.usf.edu)

Z. Lee, Department of Environmental, Earth and Ocean Sciences, University of Massachusetts, Boston, MA 02125, USA.